AD-A179 527 PLASMA THEORY AND SIMULATION(U) CALIFORNIA UNIV 1/1
BERKELEY ELECTRONICS RESEARCH LAB C K BIRDSALL
31 DEC 85 N00014-85-K-0089

UNCLASSIFIED F/G 20/9 NL

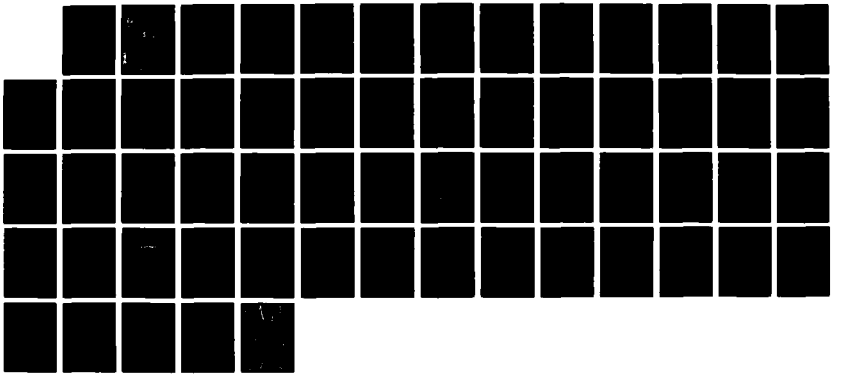

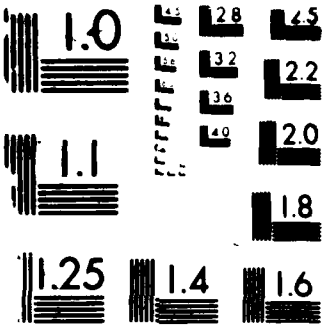

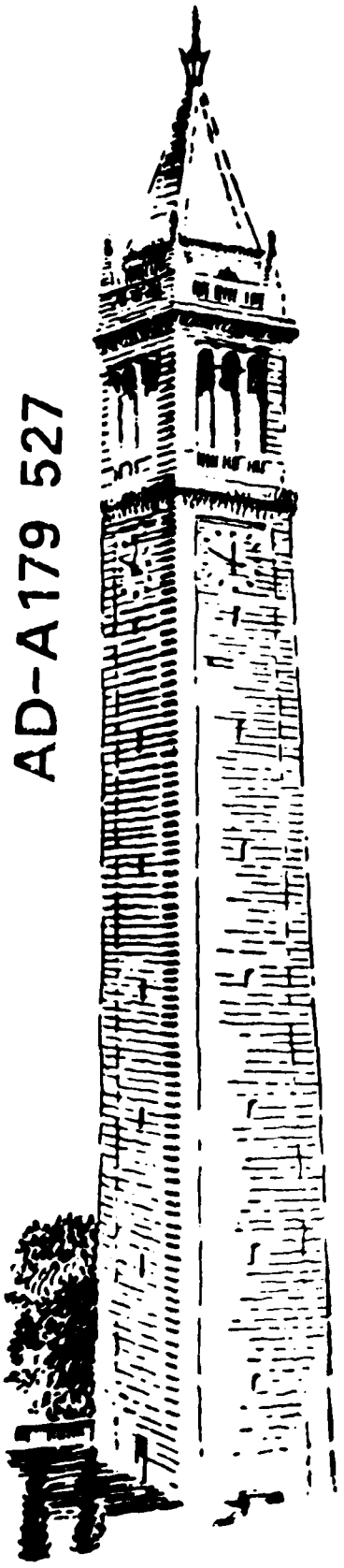

THIRD & FOURTH QUARTER PROGRESS REPORT 1985

ON PLASMA THEORY AND SIMULATION

July 1 to December 31, 1985

DOE Contract DE-AT03-76ET53064
ONR Contract N00014-85-K-0809
Varian Gift and MICRO
Hughes Aircraft Co. Gift

ELECTRONICS RESEARCH LABORATORY
College of Engineering
University of California, Berkeley, CA 94720

SECURITY CLASSIFICATION OF THIS PAGE (When Data Entered)

REPORT DOCUMENTATION PAGE	READ INSTRUCTIONS BEFORE COMPLETING FORM
1. REPORT NUMBER	2. GOVT ACCESSION NO. AD-A179 527	3. RECIPIENT'S CATALOG NUMBER
4. TITLE (and Subtitle) Quarterly Progress Report III, IV July 1, 1985 - Dec. 31, 1985	5. TYPE OF REPORT & PERIOD COVERED Progress, 7/1-12/31, 1985 6. PERFORMING ORG. REPORT NUMBER
7. AUTHOR(s) Professor Charles K. Birdsall	8. CONTRACT OR GRANT NUMBER(s) ONR N00014-85-K-0809
9. PERFORMING ORGANIZATION NAME AND ADDRESS Electronics Research Laboratory University of California Berkeley, CA 94720	10. PROGRAM ELEMENT, PROJECT, TASK AREA & WORK UNIT NUMBERS Element No. 61153N, Project Task Area RR01-09-01, Work Unit No. NR 012-742
11. CONTROLLING OFFICE NAME AND ADDRESS ONR Physics Division Department of the Navy, ONR Arlington, VA 22217	12. REPORT DATE 13. NUMBER OF PAGES
14. MONITORING AGENCY NAME & ADDRESS(if different from Controlling Office)	15. SECURITY CLASS. (of this report) Unclassified 15a. DECLASSIFICATION/DOWNGRADING SCHEDULE

16. DISTRIBUTION STATEMENT (of this Report)

Approved for public release; distribution unlimited

17. DISTRIBUTION STATEMENT (of the abstract entered in Block 20, if different from Report)

18. SUPPLEMENTARY NOTES

Our group uses theory and simulation as tools in order to increase the understanding of plasma instabilities, heating, transport, plasma-wall interations, and large potentials in plasmas. We also work on the improvement of simulation both theoretically and practically.

19. KEY WORDS (Continue on reverse side if necessary and identify by block number)

Research in plasma theory and simulation, plasma-wall interactions, large potentials in plasmas

20. ABSTRACT (Continue on reverse side if necessary and identify by block number)

See reverse side

DD FORM 1 JAN 73 1473 EDITION OF 1 NOV 65 IS OBSOLETE
S/N 0102-LF-014-6601

Unclassified
SECURITY CLASSIFICATION OF THIS PAGE (When Data Entered)

20. ABSTRACTS

General Plasma Theory and Simulation

A. Linear magnetized plasma response to an oblique electrostatic wave. Trapping and resonant heating are observed.

B. Limits of linear response of a Vlasov distribution. Final report issued.

C. Saturation and post-saturation behavior of the Alfven ion-cyclotron instability: A simulation study. (Final report issued) Quasilinear diffusion observed; ion trapping also observed, important in saturation.

D. Stabilizing effects of finite-amplitude RF waves on the interchange instability. (Final report issued) An exact energy conservation law is developed. No stabilization of the incompressible interchange mode occurs unless the RF wave has a k_{11}.

*E. Effect of large amplitude perpendicularly-propagating RF waves on the interchange instability. (Final report issued) Only modest corrections to the interchange growth rates are found.

*F. Numerical simulations of turbulent trapping in the weak beam-plasma instability: Study of the growth rates. (Memorandum issued) Growth rates were found to be enhanced over the quasilinear models, but smaller than from the turbulent trapping model.

Plasma-Wall Physics, Theory and Simulation

**A. Planar magnetron discharge simulations. This 1½d model shows ion sheath Child's Law behavior and return of electrons at the sheath edge.

B. Planar magnetron discharges: Mechanisms for instability, and numerical study of equilibrium. This study is in 2d, covering diocotron and Kelvin-Helmholtz instabilities, some theory, and some initial results.

Code Development and Software Distribution

A. ES2: An electrostatic 2d bounded simulation code with injection and external circuit. Initial results for the 2½d plasma magnetron are shown.

B. Energy conserving reflection algorithm. The questions of making reflection of particles conserve energy are addressed and solved.

Major support is from DOE.
*Supported in part by ONR.
**Supported in part by Varian/MICRO.

THIRD AND FOURTH QUARTER PROGRESS REPORT
ON
PLASMA THEORY AND SIMULATION

July 1 to December 31, 1985

Our research group uses both theory and simulation as tools in order to increase the understanding of instabilities, heating, transport, plasma-wall interactions, and large potentials in plasmas. We also work on the improvement of simulation, both theoretically and practically.

Our staff is -

Professor C. K. Birdsall Principal Investigator	191M	Cory Hall	(643-6631)
Dr. Kim Theilhaber Post-Doctorate	187M	Cory Hall	(642-3477)
Dr. Ilan Roth (part-time) Research Physicist, Space Science Lab, UCB	187M	Cory Hall	(642-1327)
Dr. Bruce Cohen	L630	LLNL	(422-9823)
Dr. A. Bruce Langdon	L472	LLNL	(422-5444)
Dr. William Nevins Adjunct Lecturers, UCB; Physicists LLNL	L630	LLNL	(422-7032)
Mr. Perry Gray Senior Engineering Aide	119ME	Cory Hall	(642-3528)
Mr. William Lawson Mr. Niels Otani Ms. Lou Ann Schwager Research Assistants	119MD 119ME	Cory Hall Cory Hall	(642-1297) (642-3528)

December 31, 1985

DOE Contract DE-AT03-76ET53064
ONR Contract N00014-85-K-0809
Varian and MICRO Gift
Hughes Aircraft Co. Gift

ELECTRONICS RESEARCH LABORATORY

University of California
Berkeley, California 94720

TABLE OF CONTENTS

Major support is from DOE.

*Supported in part by ONR.

**Supported in part by Varian/MICRO

SECTION I: GENERAL PLASMA THEORY AND SIMULATION

A. Linear Magnetized Plasma Response to an Oblique Electrostatic Wave

William S. Lawson

Abstract

The linear response of a spatially periodic magnetized Vlasov plasma distribution function is computed to second order in the electric field. The results for a specific electric field are then compared with the results of computer simulation for different amplitudes of the electric field. Both trapping and resonant heating are observed, and both appear to contribute (for the chosen parameters) to limiting the validity of linear theory at larger electric field amplitudes.

This is to be issued as ERL Memo No. UCB/ERL M86/94, Dec. 15, 1986. The abstract follows.

B. Limits of Linear Response of a Vlasov Distribution

William S. Lawson

The abstract for this appeared in the previous QPR. The report is being issued as ERL Memo No. UCB/ERL M86/44, June 3, 1986.

C. Saturation and Post-Saturation Behavior of the Alfven Ion-Cyclotron Instability: A Simulation Study

Niels F. Otani

This is to appear as ERL Memorandum No. M86/15, Feb. 19, 1986. The abstract follows.

D. Stabilizing Effects of Finite-Amplitude RF Waves on the Interchange Instability

Niels F. Otani

This is to appear as ERL Memorandum No. UCB/ERL M86/18, Feb. 28, 1986. The abstract follows.

E. Effect of Large-Amplitude Perpendicularly-Propagating RF Waves on the Interchange Instability

Neils F. Otani and Bruce I. Cohen

This is to appear as ERL Memorandum No. UCB/ERL M86/48, July 8, 1986. The abstract follows.

F. Numerical Simulations of Turbulent Trapping in the Weak Beam-Plasma Instability: Study of the Growth Rates

Dr. Kim Theilhaber

This work will be issued in an ERL Memorandum, "Numerical Simulations of Turbulent Trapping in the Weak Beam-Plasma Instability," by K. Theilhaber, ERL Memo M86/50, June 5, 1986. The abstract follows.

Saturation and Post-Saturation Behavior of the Alfvén Ion-Cyclotron Instability: A Simulation Study

Niels F. Otani
Electronics Research Laboratory
University of California
Berkeley, California 94720

Two computer codes based on different algorithms are employed in the study of the Alfvén ion-cyclotron instability. Features of quasilinear diffusion are clearly exhibited and identically modeled by the two codes. Ion trapping is also observed and appears to play an important role in the saturation process. Relaxation of the anisotropy in the ion temperature and transverse wave energy transfer from intermediate to long wavelength modes are observed to proceed more slowly following instability saturation when the possibility of nonlinear $\mathbf{E} \times \mathbf{B}$ electrons is allowed, and more slowly still when longitudinal ion sound modes are present. Fluctuations in the short wavelength modes are shown to be a discrete particle effect, with levels agreeing with predictions calculated from a test-particle model.

Stabilizing Effects of Finite-Amplitude RF Waves on the Interchange Instability

Niels F. Otani
Electronics Research Laboratory
University of California
Berkeley, California 94720

The effects of the presence of a finite-amplitude RF wave on the interchange instability are studied theoretically in a three-dimensional quasineutral Darwin two-fluid system. An exact energy conservation law is developed for the system equations. The perturbed dynamical quantities are expanded to second order in the fluid displacements and it is demonstrated that a Lagrangian exists for the system. The interchange perturbation energy is calculated and terms associated with the perturbed magnetic potential energy are analyzed. For the terms studied, it is found that no stabilization of the incompressible interchange mode occurs unless the RF wave has a parallel-propagating component, and that coupling to perpendicular-propagating sidebands does not influence the stability of perpendicularly-propagating interchange modes. The stabilizing influence of these terms also does not depend directly on the presence of RF field gradients. The analysis suggests a physical mechanism by which RF stabilization can occur—the RF wave stabilizes the interchange mode by forcing the mode to bend magnetic field lines.

Effect of Large-Amplitude Perpendicularly-Propagating RF Waves on the Interchange Instability

Niels F. Otani*
Electronics Research Laboratory
University of California
Berkeley, California 94720

Bruce I. Cohen
Lawrence Livermore National Laboratory
University of California
Livermore, California 94550

Results are presented from hybrid 2-d quasineutral Darwin simulations of the interchange instability in the presence of a large RF wave in the ion-cyclotron frequency range. The simulation models the plane perpendicular to the background magnetic field using cold, particle ions and a cold $\mathbf{E} \times \mathbf{B}$ electron fluid. Related theory is also discussed. Fluid equations appropriate to our simulation model are derived and their properties demonstrated and compared to simulation. A method for solving for the RF-modified growth rates from the fluid equations is described. It is generally expected that the current component associated with the mean, RF-induced ion drift is capable of influencing the stability of the interchange mode; however, no modification of the mean ion drift is observed in simulations in which RF is present. Instead, in both the theory and simulation, an *electron RF-field* oscillation current dominates the modification to the gravitational current. As a result, even in the presence of large RF fields, ($B_{RF}/B_0 = 15\%$) only modest corrections to the interchange growth rates are observed. The effect is stabilizing for $kL_n \lesssim 0.8$–0.9, apparently for both signs of the square-electric-field gradient, and is destabilizing for larger values of kL_n, although the credibility of the simulation begins to become suspect here. Fractional reduction of the interchange growth rate is observed to be quadratically dependent on the RF wave amplitude, independent of ion-cyclotron resonant effects, and proportional to $\nabla B_{RF}^2/\nabla B_0^2$, consistent with an eikonal theory developed for the study of stabilizing effects on perpendicularly-propagating fast Alfvén waves. The results also suggest that additional gradient-independent stabilizing effects may be operative when $kL_n \sim 1$. Finally, it is also observed that, while the RF wave has little effect on the interchange instability, the interchange mode strongly affects the RF wave, damping it significantly as the mode saturates.

* Present address: Courant Institute of Mathematical Sciences, New York University, New York, New York 10012.

NUMERICAL SIMULATIONS OF TURBULENT TRAPPING IN THE WEAK BEAM-PLASMA INSTABILITY: STUDY OF THE GROWTH RATES

K. Theilhaber
Plasma Theory and Simulation Group
Electronics Research Lab
University of California
Berkeley, CA 94720 USA

G. Laval and D. Pesme
Centre de Physique Theorique
Ecole Polytechnique
91128 Palaiseau, France

ABSTRACT

Numerical simulations of the weak beam-plasma instability were done in the turbulent regime where small-scale trapping is a dominant feature of the instability, a regime with behavior not predicted by quasilinear theory. It occurs when the trapping frequency $v = (k^2D)^{1/3}$ is larger than the growth rate γ_k of the instability. The results of the simulations were compared with those of a specific model of the turbulence, the so-called "turbulent trapping" model, which predicts a growth rate well enhanced over the quasilinear value. It was found that while growth rates were enhanced over the quasilinear values, the enhancements observed are smaller than expected from the quantitative predictions of the model. Further work is necessary to determine whether this discrepancy is a failing of the turbulent trapping model, or the result of the numerical limitations of our computational scheme.

SECTION II: PLASMA-WALL PHYSICS, THEORY AND SIMULATION

A. Planar Magnetron Discharge Simulations

Perry Gray (Prof. C. K. Birdsall)

A one-dimensional particle plasma simulation code, following the self-consistent motion of thousands of particles, has been developed to complement theory and experiment in studies of plasma-sheath and sheath-wall interactions, for a variety of applications with respect to plasma-assisted materials processing problems.

We have implemented volume generation of ions and electrons (in contrast to the surface emission model described earlier). The ionization rate can be made a function of some local variable (e.g., local electric field or electron density). We have also added transport diagnostics in the form of fluxes (particle, kinetic energy, and heat) and temperature as functions of x and secondary emission from the cathode surface. We will add to the model the effects of charge-neutral collisions. The bounce motion of the particles, from mirror to mirror, may be added. With these additions, we believe that much of the essential physics of the crossed field discharges will be modeled. Initial simulation studies of the discharge have been performed.

The first simulation studies performed use the one-dimensional (1-d, 3-v) model of the planar magnetron shown in Figure 1. The ignorable directions are y and z. The dimension of the simulation is a cut along x, the axis of symmetry, so that the magnetic field is perpendicular to the direction of simulation. We keep track of velocities in all three directions so that gyromotion of the ions and electrons is included. The magnetic field B_z (x) is assumed to be due to a linear dipole, offset with respect to the right boundary of the simulation as shown, or to be uniform. The left boundary of the simulation is at ground ($\phi = 0$), while the right boundary has a fixed d.c. bias (and may also be a.c. driven).

Typical laboratory parameters are:

$$kT_e = 5eV, kT_i = 0.025eV \quad (T_i << T_e, \text{ essentially cold ions})$$

$$n_i \cong n_e = 10^{12}/cm^3$$

$$B_z = 1kG$$

which produces:

$$\omega_{pe} \approx 6 \times 10^{10} \text{ sec}^{-1}, \omega_{ce} \approx 1.8 \times 10^{10} \text{ sec}^{-1}$$

$$v_{te} \approx 10^8 cm/sec, \quad \lambda_{De} \quad 1.6 \times 10^{-3} cm$$

Let V_o = -100 volts (eV_o/kT_e = -20)

Typical gas is argon, with $m_i \cong 40m_{proton} \cong 73{,}000m_e$

For the simulation model, we are forced to use much smaller mass ratios, in order to follow fast (electron) and slow (ion) time scales. We also use a far smaller number of particles (superparticles, each with, say, 10^{12} electrons).

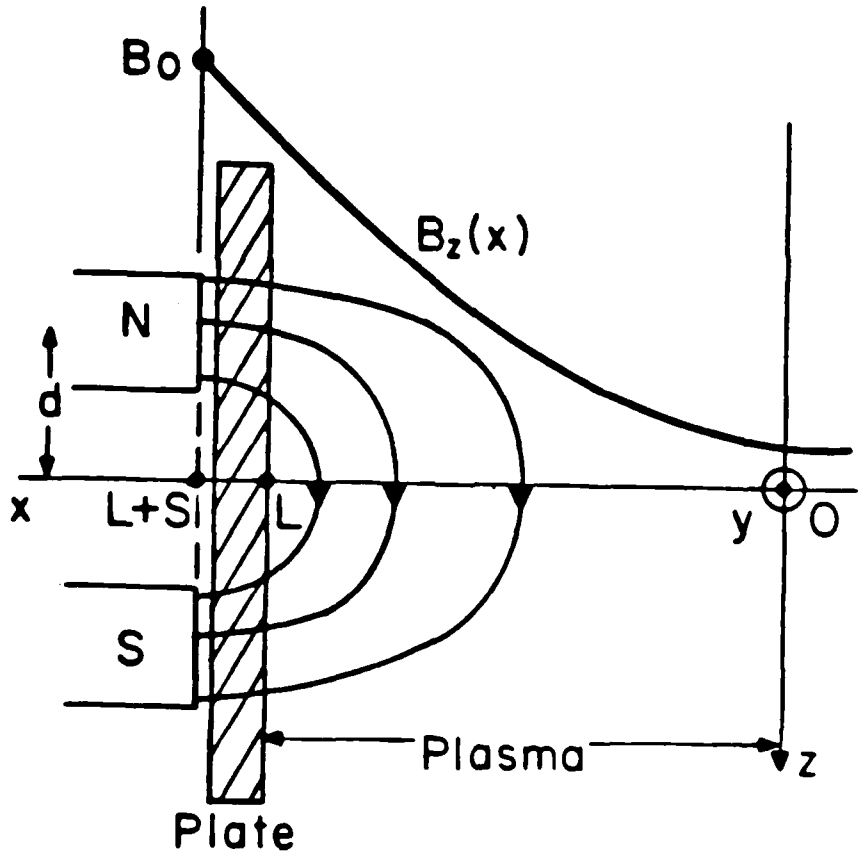

Figure 1

Typical initial results for B uniform in (x) are shown in Figure 2. The left-hand electrode is grounded ($\phi = 0$) and the right-hand electrode is held at $e\phi/kT_e = -20$. (Typical laboratory discharges have $kT_e \approx 5eV$, so this is a bias of -100 volts.) The ions are considered cold. (Typically $kT_i \approx 0.025eV$ so $T_i << T_e$.) We use a mass ratio of $m_i/m_e = 40$ so as to be able to follow both electrons and ions conveniently.

The results shown are at time $t \approx 31$ (after 4000 time steps) with roughly 2000 each of electrons and ions. The potential $\phi(x)$ remains near 0 over most at the space, then starting at $x \approx 8$ dips to $e\phi(L)/kT_e = -20$. The electrons are repelled by the positive electric field in this space $x > 8$, as observed in the v_x - x phase space plot, never reaching beyond $x \approx 8$. On the other hand, the ions, beginning at $x = 8$, are accelerated by the E_x, hitting the right hand plate with high velocity, well beyond v_{ti} (accelerated by close to the 100 volts). One quantitative feature is that the curvature of $e\phi(x)$ is negative so that the power law is $e\phi(x) \sim (x-8)^n$ with $n > 1$; similarly the curvature of the ion acceleration is like $v_i(x) \sim (x-8)^m$ with $m < 1$. The temptation is to say that $n = 4/3$, a Child's Law region, making $m = 2/3$ as the ions are accelerated nearly from rest. That is to say, the ions free-fall near the right hand electrode, influenced by E_x, as if B_z were zero. The correlation is good with experiment in that a dark space is observed next to the negative plate (where the electron population is quite low) and its length is associated with the sheath thickness, and not the ion gyroradius. The electrons have gyroradius of $a_e = v_{te}/\omega_{ce} = 1/8$ and the thermal ions have a gyroradius of $a_i = v_{ti}/\omega_{ci} = 0.005/(8/40) = 0.025$, both fairly well magnetized. Hence, how do the ions free fall, if they are so tightly bound to B_z (gyroradius small compared with L)? Note that at $x \approx 8$, the cold ions have become accelerated a little, to about $v_i \approx 0.1$ which gives a much larger a_i (by the factor $0.1/0.005 = 20$) of about 0.5; near $x = 9$ the ions are at $v_i \approx 0.5$ with again much larger $a_i \approx 2.5$ and $x = 10$, ions are near $v_i \approx 1.0$ with $a_i = 5$ (or, gyrodiameter = L, diode spacing). Hence, a_i increases dramatically, so that free fall takes place. The transport of ions needs no collisions to take place.

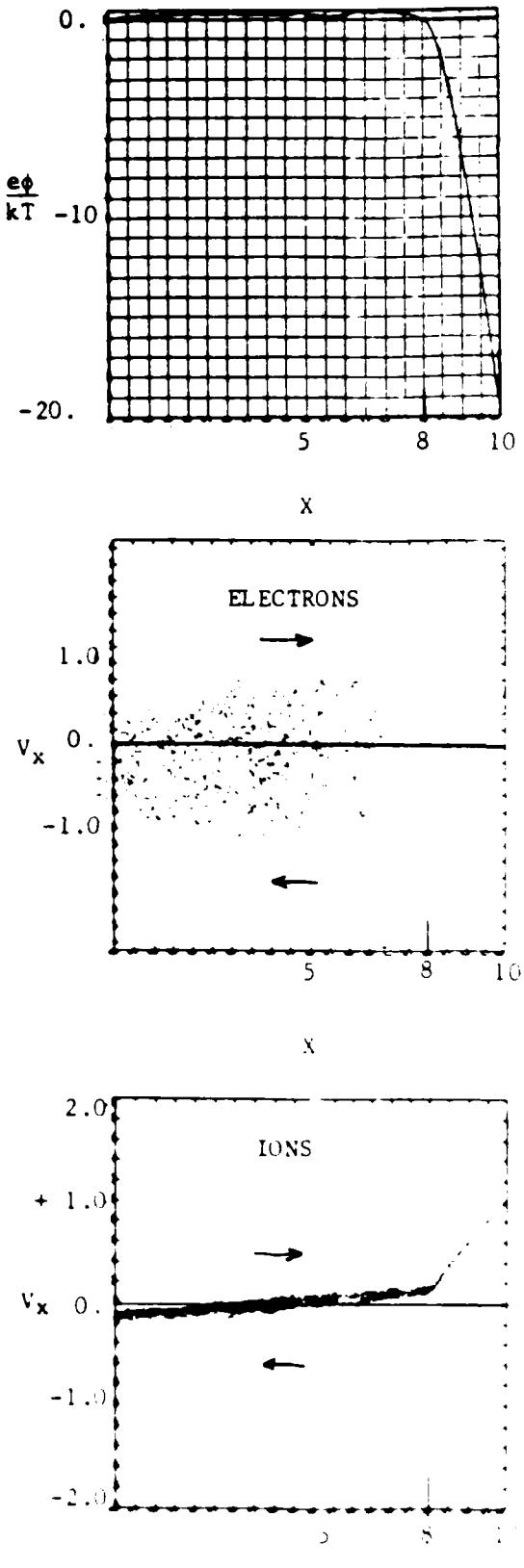

Figure 2

B. **Planar Magnetron Discharges: Mechanisms for Instability, and Numerical Study of Equilibrium – K. Theilhaber.**

1 Introduction

In the following report, we shall present a two-dimensional simulation model for the planar magnetron which embodies a plausible mechanism for instability and fluctuating behavior of the magnetron discharge. In this model, the magnetic field is perpendicular to the plane of motion of the ions and the electrons, in the so-called "crossed-field" configuration. This article is meant as a preliminary study which should help put the problem in an appropriate perspective for modelling; it includes a short review of previous work on instabilities occuring in cross-field configurations, some analytic work specific to our planar magnetron model, and numerical work on the equilibrium of this model. Our long term goal will be to simulate the entire nonlinear evolution of the two-dimensional instabilities which can occur in the planar magnetron configuration.

2 Review of Existing Crossed-Field Theory

In the past, crossed-field instabilities have been examined in at least two configurations, whose similarities with the planar magnetron geometry lead us to believe that analogous behavior will occur in the magnetron discharge as well. In both cases, the source of free energy resides in the shear of the velocity field of the particles, a shear which is induced by nonuniform $\mathbf{E} \times \mathbf{B}$ drifting perpendicular to the magnetic field. The two configurations we shall mention embody extreme examples of crossed-field instability, and we expect that the magnetron model will exhibit an instability of an intermediate type, which partakes of both extremes.

2.1 The Diocotron Instability

This is an instability which occurs in a single-species, non-uniform, non-neutral plasma, and which has been studied in connection with the behavior of electronic devices. The model of this instability allows for small space scales (thin sheets of charge, etc), and the presence of material boundaries.

The discovery of the Diocotron instability goes back to work by O. Buneman[1]. More recent work includes that of Knauer[2] and Byers[3]. The simplest configuration, which we shall discuss here, is that of a very thin charged sheet of electrons, drifting perpendicular to a magnetic field, a situation treated analytically by R. Gould in 1957 [4], who also provided a physical explanation for the instability. The dispersion relation of such a system is found to be:

$$\omega = k_y u_0 \pm i \frac{k_y \sigma_0}{2 B_0 \epsilon_0}, \tag{1}$$

whre u_0 is the mean velocity of the sheet, σ_0 its charge per unit area, B_0 the magnetic field strength, and k_y the wave-number of the perturbation parallel to the sheet and perpendicular to B. If w is the sheet thickness, and n_0 the mean electron density in the sheet, then the growth-rate can be written:

$$\gamma = \frac{1}{2} |k_y w| \frac{\omega_{pe}^2}{\omega_{ce}}, \tag{2}$$

where $\omega_{pe}^2 = n_0 e^2 / m_e \epsilon_0$, $\omega_{ce} = eB_0/m_e$, and with the thin-sheet condition, $|k_y w| \ll 1$. For $|k_y w| \sim 1$, Eq.(2) can be taken as qualitatively correct. If we assume that $\omega_{pe} \sim \omega_{ce}$, a situation possible for the magnetron discharge, Eq.(2), which models a very extreme configuration, predicts a large growth rate, $\gamma \sim \omega_{pe}$.

2.2 The MHD Kelvin-Helmholtz Instability

This is an instability which occurs in a two-species, almost neutral plasma, and which has been studied in connection with space-science problems. This model calls for large scale lengths and boundary conditions at infinity (or very far away from the shear layer).

In form, the MHD Kelvin-Helmholtz instability is closer to a pure hydrodynamic instability than the Diocotron instability. It has been studied by Chandrasekhar[5], who has given explicit analytic expressions for the growth rate, under the assumption of simple velocity shear profiles. More recent work can be found in the articles by Miura and Pritchett[6] and Pritchett and Coroniti[7]. The first reference provides a fluid treatment of the Kelvin-Helmholtz instability, with the growth rates found through a numerical integration of the fluid equations. The second reference extends the fluid analysis by presenting the results of a particle simulation, against which the predictions of the fluid picture can be checked.

In both of [6,7], the conditions assumed for the MHD model are (Fig.(1)):

1. an almost neutral plasma (in sharp contrast to the Diocotron instability).

2. infinitely magnetized electrons.

3. the dynamics are determined by the ions (as opposed to the Diocotron instability, where electrons, the only species present, determine the growth rates).

4. the ordering of the scale lengths is:

$$\rho_e \ll \rho_i \ll a \leq \lambda_y, \tag{3}$$

where (see Fig.(1)), ρ_e and ρ_i are the Larmor radii, a the width of the shear layer, and λ_y the wavelength of the perturbation parallel to the velocity direction.

With the above conditions, and with the velocity shear determined by:

$$v_{0y}(x) = -E_{0x}(x)/B_0, \tag{4}$$

where E_{0x} is the equilibrium electric field, the analysis of the fluid equations leads to a dispersion relation in which the frequency ω is obtained as a solution of the eigenvalue problem:

$$\frac{d^2}{dx^2}\delta v_{iz} - \left(k_y^2 - \frac{k_y v_{0y}''}{\omega - k_y v_{0y}}\right)\delta v_{iz} = 0, \tag{5}$$

where δv_{iz} is the velocity perturbation, with $\delta v_{iz}(\pm\infty) = 0$. Corresponding to each value of ω, Eq.(5) predicts an eigenfunction $\delta v_{iz}(x)$.

Miura and Pritchett[6] obtained the growth-rate for the shear profile:

$$v_{0y}(x) = v_0 \ \tanh(x/a), \tag{6}$$

where a determines the width of the shear layer and v_0 its magnitude. In fact, the authors of [6] did not resort to a direct solution of Eq.(5), but rather to a numerical integration in time of the system of linearized fluid equations: the resulting profile for the growth rate is shown in Fig.(2). The growth-rate has a maximum for $k_y a \approx 0.5$, for which $\lambda_y \approx 4\pi a \approx 12a$. As the eigenfunctions extend over a distance in x comparable to λ_y, the maximum growth rate occurs for velocity perturbations extending over many times the shear length. In its nonlinear stages, the instability develops vortices which are also considerably larger than the dimensions of the shear layer.

A surprising result of the particle simulations of Pritchett and Coroniti[7] is that they show that the fluid calculations outlined above are valid even when the ion gyroradius is comparable in size to the width of the shear layer, $a \sim \rho_i$ (though not when it is smaller, $a \ll \rho_i$). This is a situation where not only one expects finite-Larmor-radius effects to be large, but in which it is extremely hard to model these effects, short of writing the full kinetic equations. Thus, the particle simulations encourage us to think that the fluid formulation is a more powerful tool than a conservative estimate would lead us to believe, and that it can be used for a first estimate of growth rates in similar configurations.

3 The Magnetron Model

We shall now outline a "first" magnetron model. Our approach in defining the model is to "streamline" it as much as possible, so that in its final form

it will exhibit the crossed-field instability in the simplest form attainable, while retaining the basic physics of the process.

The first problem in designing the model is to determine the equilibrium conditions. The creation and sustenance of the magnetron discharge are thought to strongly relie on collisional processes, such as neutral ionization and secondary electron emission, which depend not only on plasma properties, but on the properties of the ambient neutral gas, and of the plate surfaces. The discharge mechanism is illustrated, in a schematic and tentative form, in Fig.(3). We believe that trying to include all of these primarily collisional effects in the model, is premature at our stage of understanding, and we thus choose to isolate the model from the detailed nature of the source mechanisms, by postulating instead *ad hoc* sources (planar or distributed) for the ions and electrons. The simplified geometry is shown in Fig.(3). As we shall see, even the choice of these given sources is not simple, as the instability mechanism is very dependent on the precise nature of the sources (injection rates, distribution in space). We are thus confronted with the problem of choosing the most plausible source condition, in the absence of a detailed understanding of the magnetron discharge.

A further simplification of the model is to concentrate on the sheath region represented in Fig.(3), across which occurs almost all of the voltage drop. Its representation in the simulation model is shown in Fig.(4). Further assumptions of the simulation model are:

1. we model only the cross-field dynamics of the sheath (in the plane perpendicular to the magnetic field).

2. the sheath plasma is a two-species, non-neutral, highly nonuniform plasma.

3. in what follows, the ion source is planar: the ions are emitted from the right-hand, high-potential plate as if from a "plasma reservoir". The ions are emitted almost cold, with $T_i \ll T_e$.

4. temporarily, we shall treat the electrons as initially distributed in the simulation region, with no subsequent electron injection.

5. the electron gyroradius is much smaller than the sheath thickness L:

$$\rho_e \ll L,$$

6. the ions' radius of curvature in falling to the collector plate is larger or of the same order as the sheath thickness L.

The model outlined above shares features of the models for the Dicotron and the MHD Kelvin-Helmholtz instabilities: it allows for a highly non-neutral, bounded plasma, but one in which the ion dynamics play an essential role.

Our approach will be to analyse the equilibrium properties of the sheath, by first removing all electrons from the system. This leads to an equilibrium which is nothing but a Child-Langmuir sheath, and for which the numerical results can easily be checked against the well-known analytic results. We shall then consider analytically the effect of a nonuniform distribution of electrons.

4 Equilibrium without Electrons: the Ion Child-Langmuir Sheath

We shall outline the analysis for the Child-Langmuir sheath, in the absence of a magnetic field, and assuming almost cold ions. We assume that the plasma "reservoir" to the right of the high-potential plate injects ions according to the flux:

$$\Gamma_i(L) = -\beta\, n_{i0} v_{ti}, \qquad \beta \equiv 1/(2\pi)^{1/2} \approx 0.4, \tag{7}$$

With the flux determined by Eq.(7), the local ion density is given by:

$$n_i(x) = \frac{\beta n_{i0} v_{ti}}{(2e/m_i)^{1/2}(V - \phi(x))^{1/2}}, \tag{8}$$

where V is the potential at the emiiting plate. We add Poisson's equation:

$$\frac{d^2}{dx^2}\phi = -\frac{e}{\epsilon_0} n_i, \tag{9}$$

and define:

$$\xi = x/L, \qquad \psi = \phi/V, \tag{10}$$

$$v_0 = (2e/m_i)^{1/2} V^{1/2}, \tag{11}$$

Then, for a monotone potential profile, we obtain the solution $\psi(\xi)$ as the solution of the implicit equation:

$$\left(K + \frac{1}{4}e_1^2\right)^{1/2}\left(K - \frac{1}{2}e_1^2\right) - \left(KF(\xi) + \frac{1}{4}e_1^2\right)^{1/2}\left(KF(\xi) - \frac{1}{2}e_1^2\right) = \frac{3}{2}K^2\,\xi, \tag{12}$$

where $F \equiv (1-\psi)^{1/2}$, and where the parameter K determines the dependence of the solution on the ion parameters:

$$K \equiv \frac{e}{\epsilon_0}\frac{\beta n_{io} L^2}{V}\frac{v_{ti}}{v_0}, \tag{13}$$

The integration constant e_1 is determined by the condition:

$$\left(K + \frac{1}{4}e_1^2\right)^{1/2}\left(K - \frac{1}{2}e_1^2\right) + \frac{1}{4}e_1^2 = \frac{3}{2}K^2, \tag{14}$$

Now for fixed voltage and sheath length, the parameter K will increase as the injection rate increases. There is a critical value of K, $K_c = 4/9 \approx 0.444$, for which $E_x = 0$ at $x = L$, and for which we get the "traditional" Child-Langmuir sheath potential and electric field profiles:

$$\phi(x) = V\left(1 - (1 - x/L)^{4/3}\right), \tag{15}$$

$$E_x(x) = -\frac{4}{3}\frac{V}{L}(1 - x/L)^{1/3}, \tag{16}$$

For $K > K_c$ (and $v_{ti} \ll v_0$), Eqs.(15,16) remain valid: injection of ions at $x = L$ has "saturated", and the excess ions are turned back to the injection plate.

5 Numerical Results for Equilibrium

We performed numerical runs of the two-dimensional, electrostatic code ES2[8], with only ions present, with the intent of checking numerical results against Eqs.(15,16). In Figs.(5,6) we show the results for the simulation with the geometry shown in Fig.(4). This configuration is unmagnetized, with $B = 0$. The plasma parameters are: $v_{ti} = 0.079$, $v_0 = (2eV/m_i)^{1/2} = 0.98$, $\epsilon = 0.01$, $\epsilon/m_i = 1/40$, and $n_{i0} = 303$. For this density of the ion reservoir, $K = K_c = 4/9$. The external circuit has $V = 19.5$ and $R = L = 0$. The agreement for the potential and electric field profiles is quite close, except near the emitting plate at $x = 10$, where the assumption of completely cold ions ($T_i = 0$) is not strictly valid. In particular, the simulation value of the electric field at the emiiting plate is nonzero, with $E_x(10) \approx -0.55$. In fact, in Fig.(7), we show that as we reduce the injected ion temperature, the current saturates to a value closer to the ideal, cold-ion saturation.

We have also studied the effect of a nonzero magnetic field. From simple kinematic arguments, one can argue for the existence of a critical magnetic field strength B_c, above which all ion current to the collector should be suppressed. This field is determined by the requirement that an ion leaving the emitter plate with zero velocity will just barely graze the collector plate before being turned back by the magnetic field. It is found to be:

$$B_c = \frac{m_i}{e} \frac{(2eV/m_i)^{1/2}}{L}, \tag{17}$$

This effect is illustrated in Fig.(8), where we show the current as a function of increasing magnetic field, with otherwise the same simulation parameters as in Fig.(5). Scatter plots of the particles in phase space are shown in Figs.(9), showing how the ion trajectories turn over with increasing magnetic field.

6 Putting In Electrons - Preliminary Theory

The electric fields predicted by Eqs.(15) or (16) are highly non-uniform across the sheath region. If we think of adding an electron population to the sheath, perhaps initially in small enough numbers so as not to notably modify the ion-sheath equilibrium, they will acquire an $\mathbf{E} \times \mathbf{B}$ motion which will be sheared in x, and this new equilibrium distribution presents the possibility of Kelvin-Helmholtz instabilities. In introducing electrons into the model, we are however faced with the difficulty of modeling their injection into the sheath region. If we attempt to inject them at the high-voltage plate, in the same manner as the ions, they will not penetrate further than a gyroradius into the simulation region, leading to an unphysical electron sheet at $x = L$. On the other hand, if we introduce the electrons as an initially localized population, say in the form of a slab, we can expect a large growth rate of the order of the "pure" Diocotron instability. Thus the electrons will be rapidly dispersed, and we suspect that dynamic behavior will cease as soon as the elctron distribution has been smeared out. Thus it would seem that to model a fluctuating steady-state, with a distributed electron population, will require a distributed and continuous creation of electrons in the sheath region. In what follows, we shall merely present a tentative theory for the initial-value problem, in which a small electron population is initially added to the ion-sheath.

We assume that the initial electron density distribution is of the form,

$$n_0(x) = N_0 + N_1 \frac{x}{L}, \tag{18}$$

and that the equilibrium electric field $E_0(x)$ is known as well, so that the equilibrium drift velocities of the electrons are given by:

$$v_{0_y}(x) = E_0(x)/B_0, \tag{19}$$

We shall use the continuity equation:

$$\frac{\partial n}{\partial t} + \nabla \cdot (n\mathbf{v}) = 0, \tag{20}$$

the momentum equation, which reduces to:

$$\mathbf{v} = \frac{\mathbf{E} \times \mathbf{z}}{B_0}, \tag{21}$$

and the Poisson equation,

$$\nabla^2 \phi = \frac{en}{\epsilon_0}, \tag{22}$$

where n refers to the electron dynamics. We assume for the moment ion-independent dynamics.

If we linearize according to:

$$n = n_0(x) + n_1, \tag{23}$$

$$\mathbf{v} = \mathbf{v}_0 + \mathbf{v}_1, \tag{24}$$

then, using the fact that $\nabla \cdot \mathbf{v}_1 = 0$, we find:

$$(\partial_t + v_{0y}\partial_y) n_1 = -v_{1x} \frac{dn_0}{dx}, \tag{25}$$

$$v_{1x} = E_{1y}/B_0, \tag{26}$$

$$E_{1y} = -\partial_y \phi_1, \tag{27}$$

$$\partial_x^2 \phi_1 = \frac{e}{\epsilon_0} n_1, \tag{28}$$

This system of equations reduces to:

$$\frac{\partial^2 \phi}{\partial x^2} - \left(k_y^2 - \frac{(k_y e n_0'/\epsilon_0 B_0)}{\omega - k_y v_{0y}} \right) \phi_1 = 0, \tag{29}$$

where the prime denotes differentiation with respect to x. With $\omega_{p1}^2 \equiv e^2 N_1 / M_e \epsilon_0$, and with:

$$M \equiv \frac{k_y}{L} \frac{\omega_{p1}^2}{\omega_{ce}}, \tag{30}$$

$$\Omega(x) \equiv \omega - k_y v_{0y}(x), \tag{31}$$

Eq.(29) takes the form:

$$\frac{\partial^2 \phi}{\partial x^2} - \left(k_y^2 - \frac{M}{\Omega(x)} \right) \phi_1 = 0, \tag{32}$$

where M is constant. Eq.(29) has no obvious analytical solutions, and it would seem that an approach analogous to that of [6], with the numerical integration in time of Eqs.(25-28) to determine the growth rate, might be preferable to a direct attack on Eq.(32). However, we shall close this Section by suggesting a variational approach to the solution of Eq.(32). If we write:

$$\psi(x) \equiv \phi(x)/\Omega(x), \tag{33}$$

then Eq.(32) takes the self-adjoint form:

$$\frac{d}{dx}\left(\Omega^2 \frac{d\psi}{dx} \right) + \Omega \left(\Omega'' - k_y^2 \Omega + M \right) = 0, \tag{34}$$

Multiplying Eq.(34) by ψ^* one then obtains a quadratic equation:

$$A\omega^2 + B\omega + C = 0, \tag{35}$$

where:

$$A = \int_{-\infty}^{\infty} dx \left(\left| \frac{d\psi}{dx} \right|^2 + k_y^2 \left| \psi \right| 2 \right), \tag{36}$$

$$B = -2k_y \int_{-\infty}^{\infty} dx \left| \frac{d\psi}{dx} \right|^2 v_{0y}(x) \tag{37}$$

$$- \int_{-\infty}^{\infty} dx \left| \psi \right|^2 \left(M - k_y v_{0y}''(x) + 2k_y^3 v_{0y}(x) \right), \tag{38}$$

$$C = \int_{-\infty}^{\infty} dx \; k_y^2 v_{0y}^2(x) \left| \frac{d\psi}{dx} \right|^2 \tag{39}$$

$$+ \int_{-\infty}^{\infty} dx \left| \psi \right|^2 k_y v_{0y}(x) \left(M - k_y v_{0y}''(x) + 2k_y^3 v_{0y}(x) \right), \tag{40}$$

Eq.(35) is in fact a variational principle for the eigenfrequency ω. One can then show that the condition $C < 0$ for all possible trial functions ψ is a sufficient condition for stability. However, the expression for C is certainly not negative definite, and we can presume that Eq.(35) has unstable roots.

7 Conclusion and Future Work

We have outlined above the framework for numerical and analytic (or semi-analytic) work on cross-field instabilities in a configuration which models part of the planar magnetron. Our basic magnetron model is not yet complete, the remaining problem lies in defining a physically meaningful electron distribution, one which presumably can supply a constant source of free energy to the Kelvin-Helmholtz instability, and which is plausible in regard to the complex collisional and ionization mechanisms suspected of generating the initial magnetron discharge. This, along with particle simulations in the dynamic regime, will be the subject of future work.

References

[1] O. Buneman, C.V.D. Report Mag. **37** (1944); and J. Electronics, **3**, 1 (1957).

[2] W. Knauer, J. of Applied Physics, **37**, 2 (1966).

[3] J.A. Byers, Phys. Fluids, **9**, 1038 (1966).

[4] R. W. Gould, J. of Applied Physics, **28**, 5 (1957).

[5] S. Chandrasekhar, *Hydrodynamic and Hydromagnetic Stability*, Oxford, at the Clarendon Press, 1961.

[6] A. Miura and P.L. Pritchett, J. of Geo. Res., **87**, A9, 7431 (1982).

[7] P.L. Pritchett and F.V. Coroniti, J. of Geo. Res., **89**, A1, 168 (1984).

[8] K. Theilhaber, "*ES2: an Electrostatic 2d Bounded Plasma Simulation Code with Injection and an External Circuit*", in the present Quarterly Progress Report.

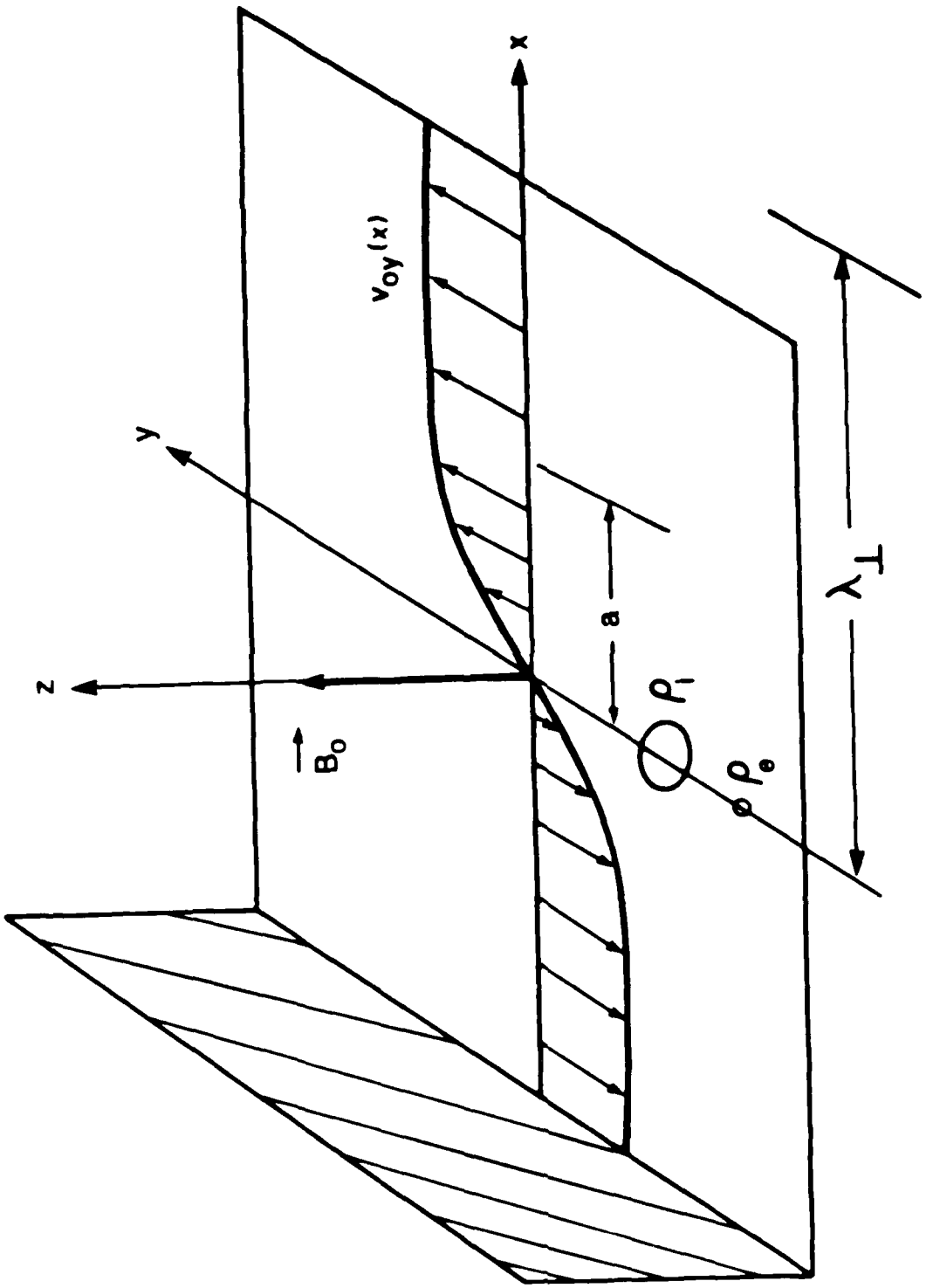

Figure 1: Geometry for the MHD Kelvin-Helmholtz instability.

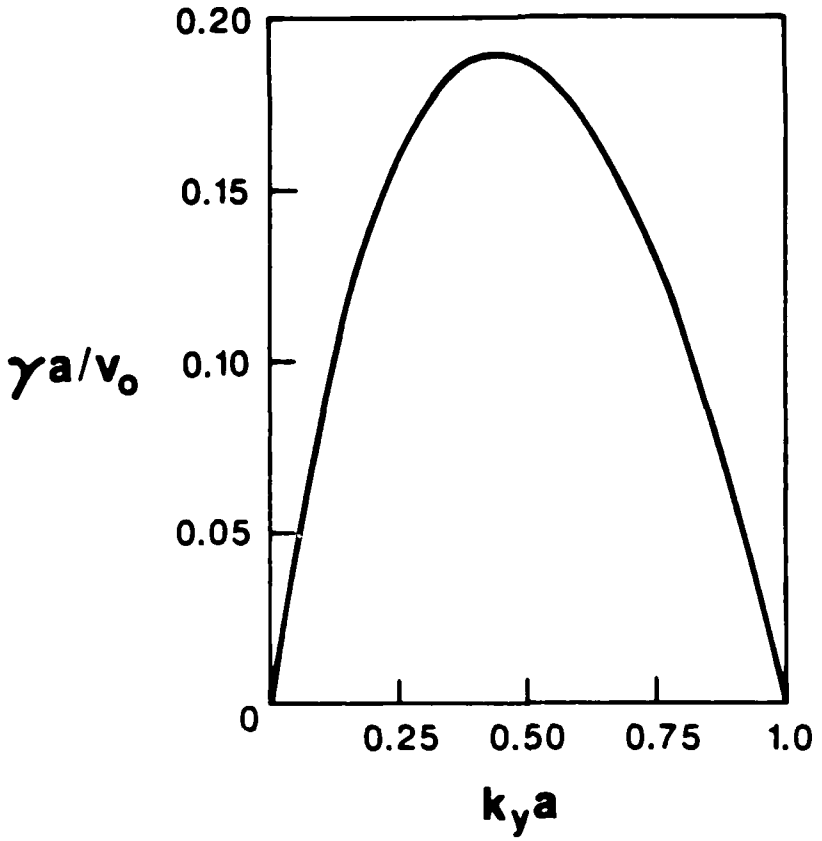

Figure 2: Growth rate of the MHD Kelvin-Helmholtz instability for the shear layer profile $v_{y0}(x) = v_0 \tanh(x/a)$ (copied from Ref.(7)).

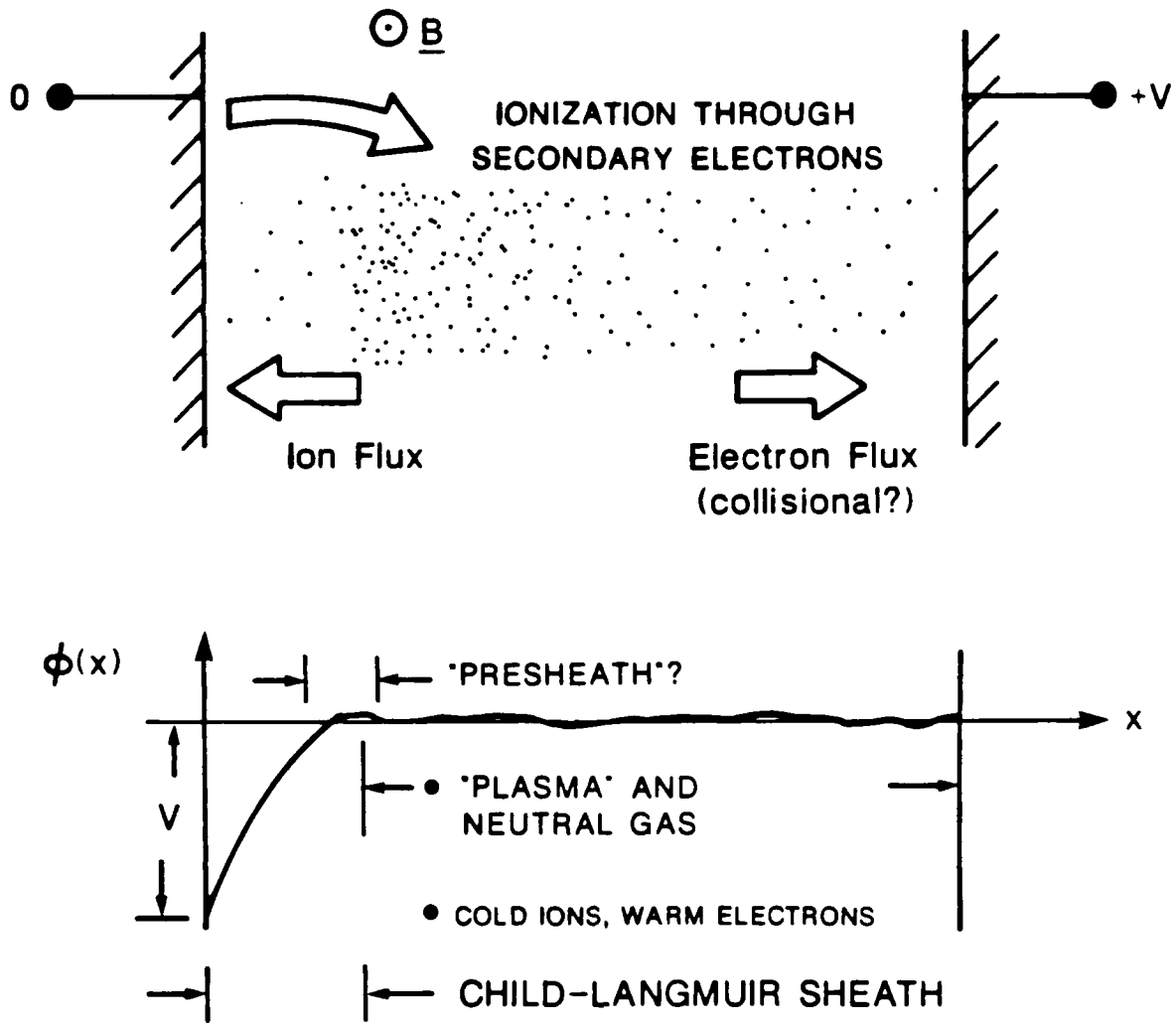

Figure 3: Schematic of the planar magnetron discharge, suggesting generation mechanisms.

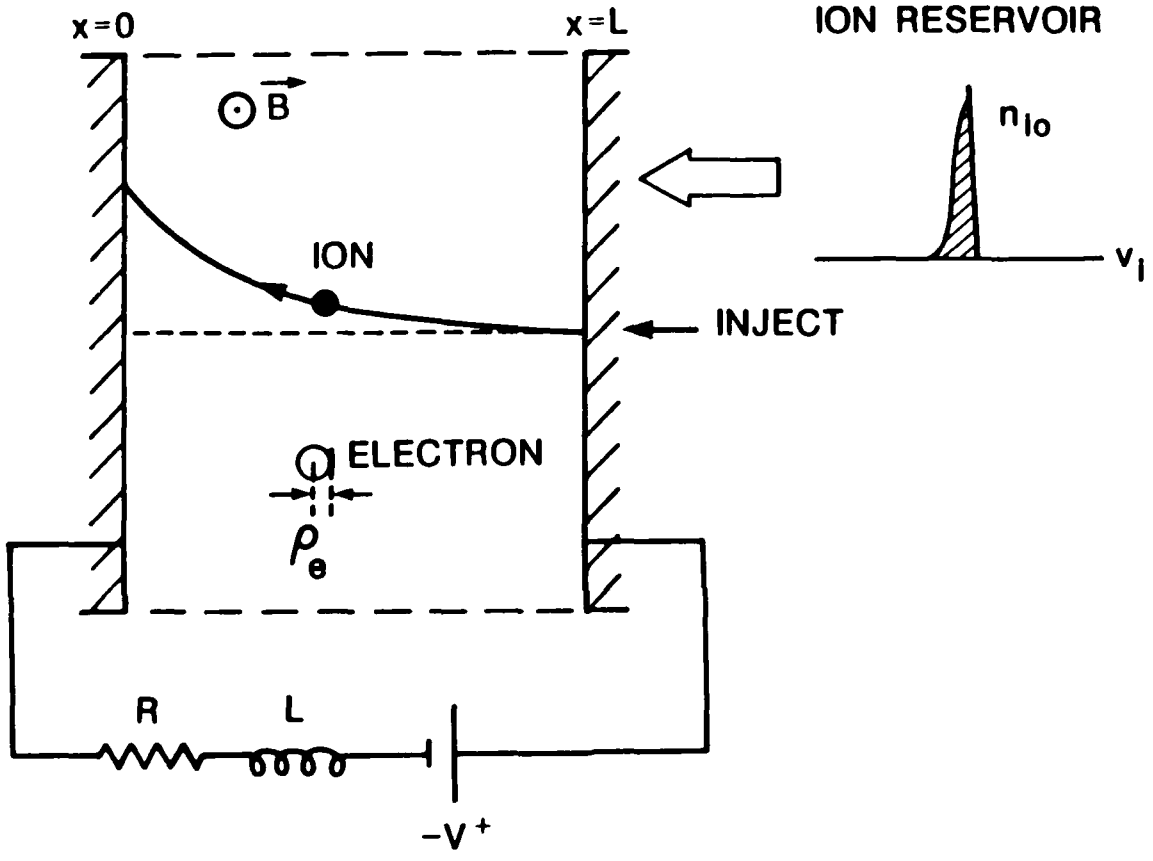

Figure 4: Idealized geometry for the planar magnetron discharge.

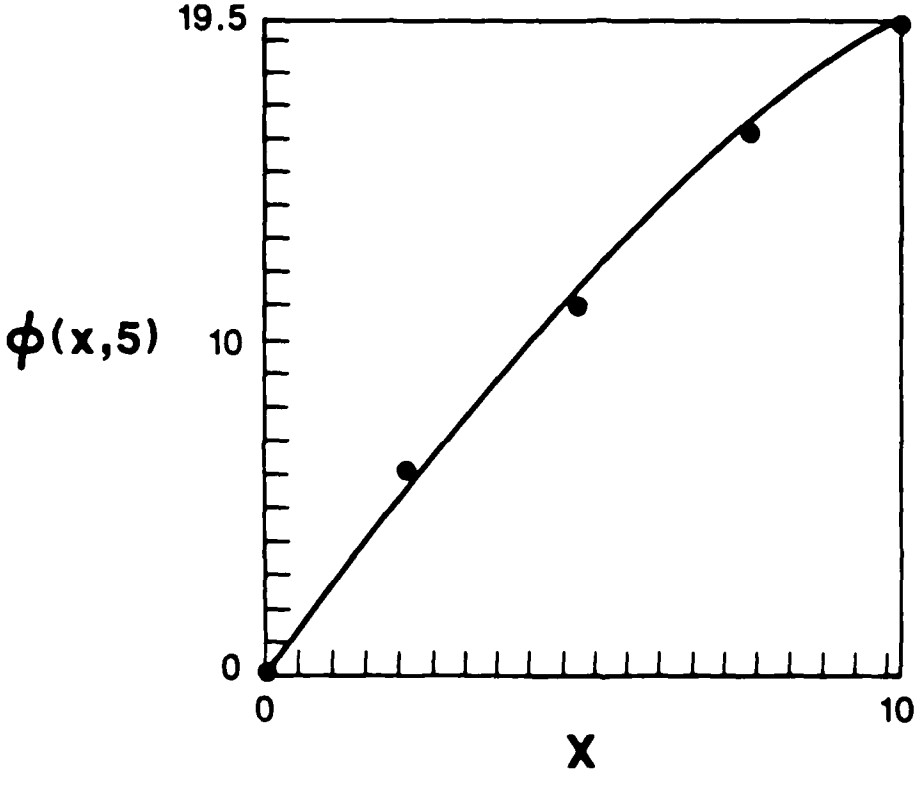

Figure 5: Potential profile for an ES2 simulation of the planar magnetron, just at saturation, $K = K_c = 4/9$. The parameters are given in the text. *Full line*: simulation result, *Dots*: analytic result, Eqs.(15).

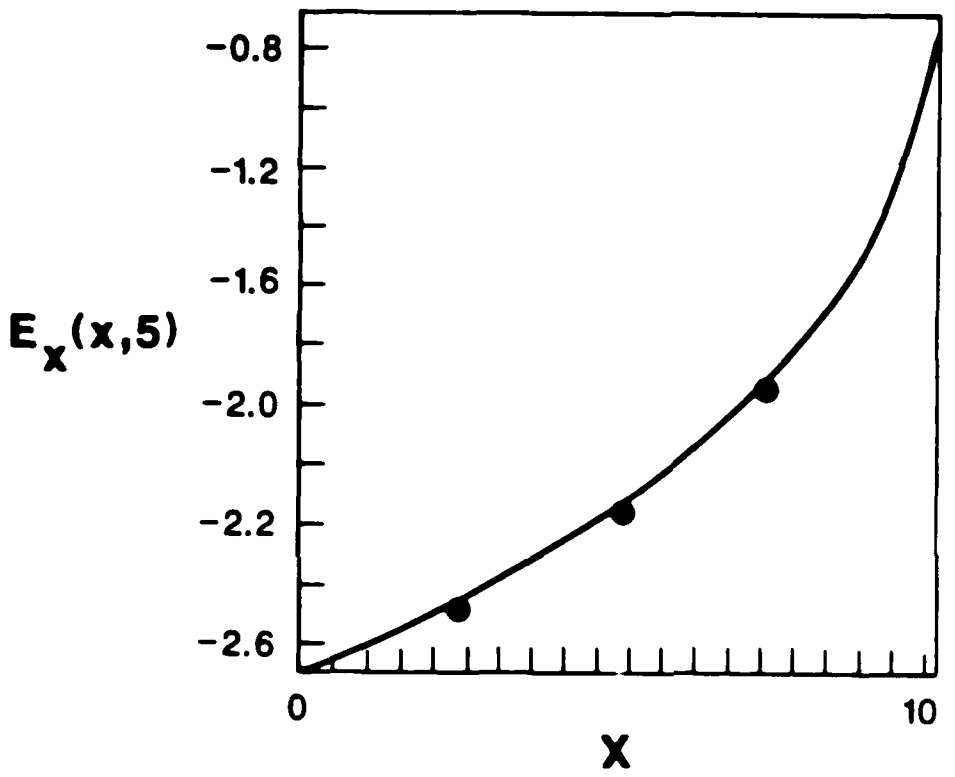

Figure 6: Electric field profile for an ES2 simulation of the planar magnetron, with the same parameters as in Fig.(5). *Full line*: simulation result, *Dots*: analytic result, Eqs.(16).

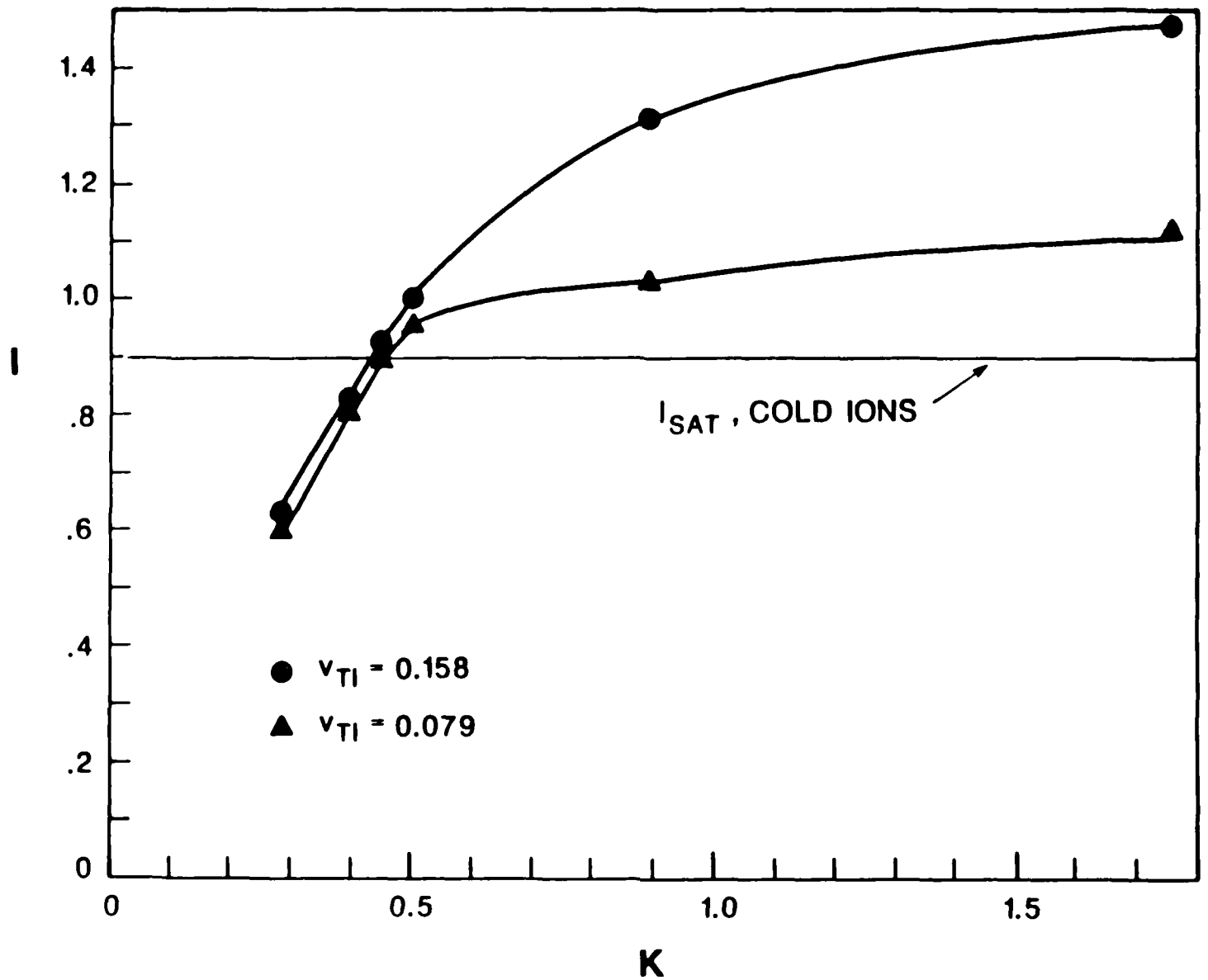

Figure 7: Current versus voltage with the parameters of the simulation of Fig.(5). We consider two ion temperatures, with n_{i0} adjusted to keep the injection rate constant, at $K = K_c = 4/9$.

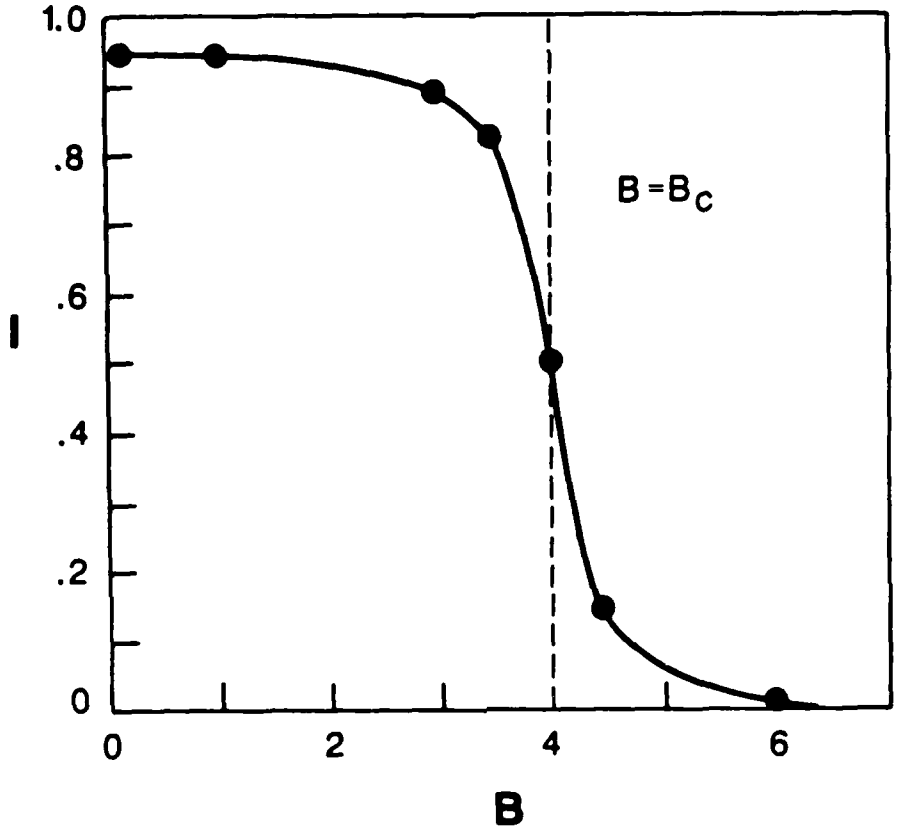

Figure 8: Current versus magnetic field, for the same parameters as in Fig.(5). The value of the critical field, $B_c = 4.0$, is found from Eq.(17).

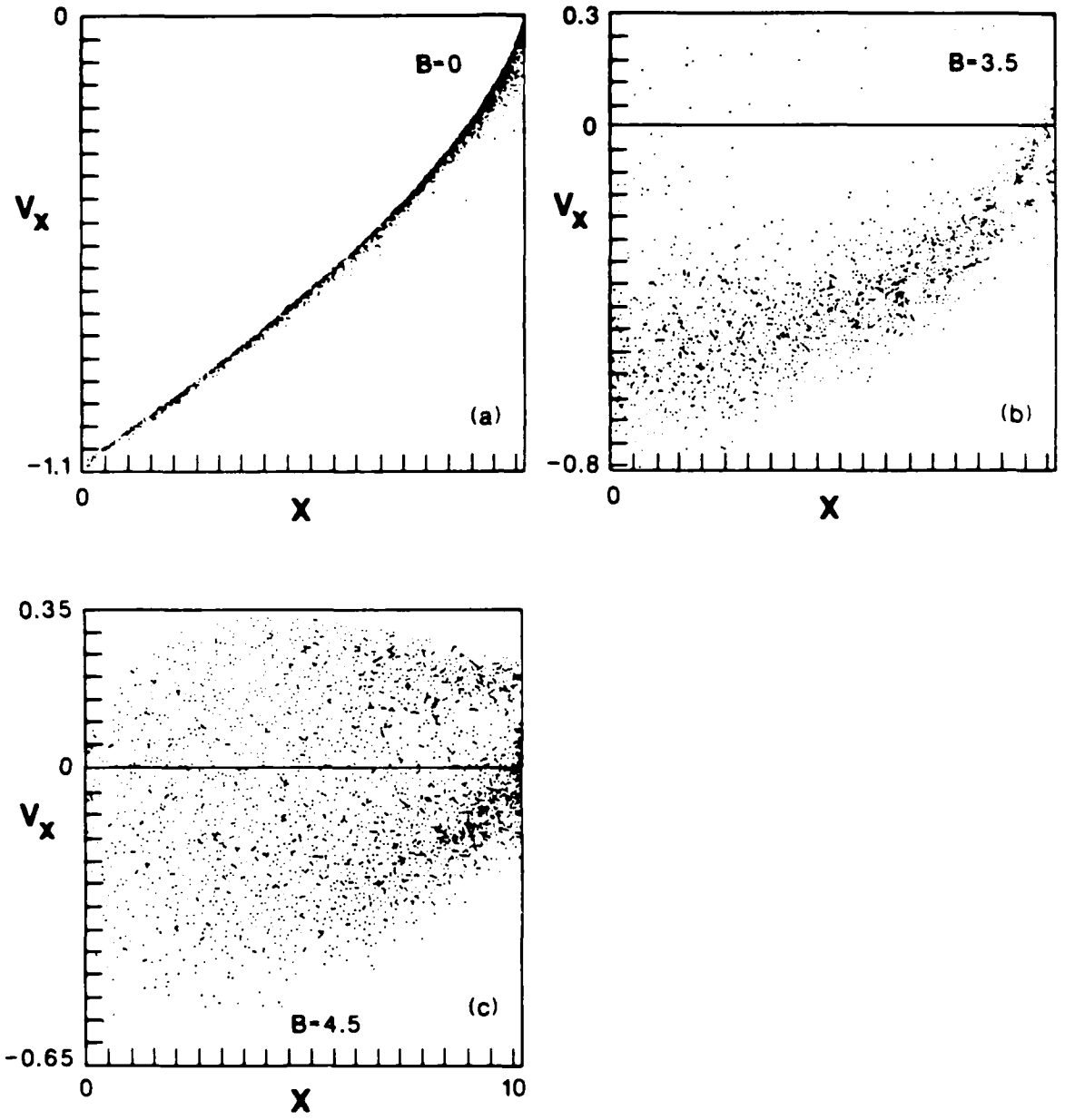

Figure 9: Ion scatter plots, v_{x_i} versus x_i, for varying magnetic fields. The critical field is $B_c = 4.0$, the other parameters are the same as in Fig.(5); (a) $B = 0$, (b) $B = 3.5$, (c) $B = 4.5$.

SECTION III: CODE DEVELOPMENT AND SOFTWARE DISTRIBUTION

Codes which we have developed or modified here are, generally speaking, available for the asking. We are making arrangements with our Industrial Liaison Program to handle distribution, at cost, of listings, tapes and/or diskettes. In a later report we will provide a list of codes and related material available and how to obtain such. If you use those, we simply ask that you acknowledge the source and also send us your results as published in reports or journals.

(Not all of the codes mentioned in our reports are available for distribution; some are single-purpose, single-user, too stylized for outside use.)

A. ES2: An Electrostatic 2d Bounded Simulation Code with Injection and External Circuit - K. Theilhaber.

I. INTRODUCTION.

The particle simulation code ES2 has been designed as a two-dimensional generalization of the one-dimensional, bounded electrostatic code PDW1([1]), and imitates or is inspired by many features of this one-dimensional code. It consists of a bounded simulation region (see Fig.(1)), containing the plasma particles (electrons and ions), with periodic boundary conditions on the particles and fields in one direction (y), and finite bounding surfaces in the other, perpendicular direction (x). At the bounding surfaces, which can represent walls or plates in a physical device, or merely open boundaries in the simulation of an infinite plasma, the code allows for the emission and absorption of particles. The code can also model the presence of an external circuit, so as to permit the external flow of charge from one boundary to the other, subject to the desired circuit characteristics. The plasma simulation, while incorporating only electrostatic self-forces, also allows for an external imposed magnetic field ($\mathbf{B}_0$ in the figure), which can be set at an arbitrary angle in the xyz plane.

ES2 has been specifically designed for extending the areas of research undertaken with PDW1, in particular the study of the physics and dynamics of the sheathes and non-neutral structures which arise in plasma-wall interactions. In the MFE environment, it can run on both Cray-1's (C and D Machines), on the Cray X-MP (E Machine), and is being adapted to run on the Cray-2 (B Machine). In what follows, we shall first give a brief synopsis of the normalizations introduced in the physical model. We shall then describe the numerical scheme used in the code, and the various options available. Finally, we give an illustrative example, and note future directions of development.

II. PHYSICAL NORMALIZATIONS.

In the electrostatic approximation assumed by ES2, the plasma is entirely described by the coupled Lorentz and Poisson equations:

$$\frac{d}{dt}\mathbf{v} = \frac{q_s}{m_s}\left(\mathbf{E} + \mathbf{v} \times \mathbf{B}\right), \tag{1}$$

$$\nabla^2\phi = -\frac{e}{\epsilon_0}(n_i - n_e), \tag{2}$$

$$\mathbf{E} = -\nabla\phi, \tag{3}$$

where s is the species index, $s = e, i$, and where n_e and n_i denote the particle densities (number per unit volume). We assume singly-charged ions, so that $q_i = -q_e = e$.

In our simulation model, we choose $e/m_e = 1$, $\epsilon_0 = 1$ and we define n_i and n_e as the number of particles per unit area. Thus, the equations of motion become:

$$\frac{d}{dt}\mathbf{v} = -(\mathbf{E} + \mathbf{v} \times \mathbf{B}), \tag{4}$$

$$\frac{d}{dt}\mathbf{v} = \frac{m_e}{m_i}(\mathbf{E} + \mathbf{v} \times \mathbf{B}), \tag{5}$$

$$\nabla^2\phi = -e(n_i - n_e), \tag{6}$$

$$\mathbf{E} = -\nabla\phi, \tag{7}$$

For instance, let us consider a homogeneous simulation plasma where electrons and ions have an equilibrium density of $\overline{n}$ (per unit area), and where the electrons are initialized with thermal velocity v_{te}, the ions with thermal velocity v_{ti}, with $v_{ti} \approx (m_e/m_i)^{1/2} v_{te}$. Then the plasma and cyclotron frequencies are simply:

$$\omega_{pe} = (e\overline{n})^{1/2}, \tag{8}$$

$$\omega_{pi} = \left(\frac{m_e}{m_i}\right)^{1/2} \omega_{pe}, \tag{9}$$

$$\omega_{ce} = B, \tag{10}$$

$$\omega_{ci} = \frac{m_e}{m_i} B, \tag{11}$$

If we then choose $v_{te} = 1$ and assume $\overline{n}$ is given, then by setting $e = 1/\overline{n}$ we insure that $\omega_{pe} = 1$ and hence that $\lambda_{de} = 1$ as well. In other words, $\overline{n}$ automatically becomes the number of particles per Debye square.

III. NUMERICAL TECHNIQUES.

We shall briefly describe the numerical schemes use in ES2.

The field solver is of a mixed type, similar to the one described by Birdsall and Langdon in ([2]): Poisson's equation is solved by using a Fourier representation of the equation in the y direction, that is by transforming from y to k_y using an FFT (Fast Fourier Transform), and by solving a finite-difference scheme in the x direction for each of the Fourier components. A final inversion, from k_y to y space using the FFT, completes the solution process. The finite-difference equation for the "d.c." ($k_y = 0$) Fourier component requires a special treatment, as it must account for the surface charge that accumulates on the boundary surfaces. This treatment is in fact nearly identical to the formulation of Poisson's equation in PDW1([1]). For the higher Fourier components, the boundary conditions are zero, and the solution of the finite difference equations is slightly simpler([2]).

The numerical particles are "square" in shape, and use a straightforward area-weighting for the gather/scatter operations, as described in Ref.([3]). When the particles hit a boundary they are absorbed, and their charge is "instantaneously" dispersed as a uniform surface charge on the conductor's surface. Similarly, when a particle is injected from a surface, it leaves a "hole" of opposite charge behind, and the hole's charge contribution is equally accounted for. A repacking algorithm, copied from PDW1, periodically discards the coordinates and velocities of particles which have been absorbed by a surface, and thus keeps the total number of particles in the system at any one time within reasonable bounds of size.

The external circuit uses an algorithm similar to the one described in ([1]). It can model a voltage source, a resistor and an inductor in series, or more simply a short or an open circuit across the plasma region.

IV. OPTIONS.

Various options exist for setting up the physical conditions of a simulation. The magnetic field can be chosen at an arbitrary angle to the xyz axes. While in the present version of ES2 the magnetic field is constant, the algorithm which moves the particles can be modified for a non-uniform magnetic field. The program can be initialized with the simulation region full or empty of particles, with prescribed stationary or drifting Maxwellians. One can separately specify the injection rates of each species at each bounding surface. The distribution functions of the emitted particles are Maxwellians, with specified temperatures and drifts. One available option assumes that the simulation region bathes in a "plasma reservoir", of given density, temperature and drift velocities; the injection rate is then automatically adjusted in accordance with the reservoir parameters.

At the present time, ES2 incorporates diagnostics in the form of scatter plots, graphs of the distribution functions, field plots of the potential and electric fields (cross-sections and contours), plots of Fourier components of the fields, and time histories of energies, circuit quantities, etc. A more specialized diagnostic provides time-averaged snapshots of grid quantities.

V. AN EXAMPLE OF AN ES2 RUN.

As an example of a run of the ES2 code, we shall consider the two dimensional simulation of instability induced by a drifting population of Maxwellian electrons, in the presence of a cold ($T_i \ll T_e$) population of ions. This is the regime for the so-called ion acoustic instability, predicted by linear plasma theory. Through particle simulations, we can hope to gain insight in the nonlinear dynamics of the process (,[4],[5]).

The system dimensions, illustrated in Fig.(1), are $L_x = 32$, $L_y = 32$, with a grid spacing $\Delta x = 1.0$ and $\Delta y = 1.0$. Thus, the numerical mesh has $N_x \times N_y = 33 \times 32 = 1056$ points. The system is initially filled with equal populations of electrons and ions (about 5000 of each), with densities $n_e = n_i = 5$ per unit area, electron charge $e = 0.2$ and mass ratio $m_i/m_e = 100$. The thermal velocities are $v_{te} = 1.0$ and $v_{ti} = 0.01$, corresponding to "temperatures" $T_e = v_{te}^2 m_e = 0.2$ and $T_i = 0.02$, so that $T_i \ll T_e$. Furthermore, the electrons are initially set drifting with a velocity $v_{de} = 1.0$. With these normalizations, we find that $\omega_{pe} = 1$, $\omega_{pi} = 0.1$, $c_s = (T_e/m_i)^{1/2} = 0.1$, $\lambda_{de} = 1$. In particular, we have $L_x = L_y = 32\lambda_{de}$. Finally, in this run we chose the plasma to be unmagnetized, with $B = 0$.

The injection rates are set to those that would obtain if the simulation region bathed in a reservoir of plasma, with exactly the same parameters as those outlined above. Thus, in the absence of collisional and collective effects, the system should be in a steady state, with injection at the boundaries exactly replenishing the particles lost by absorption at these same boundaries. In fact, this is not the case: first, because even when $v_{de} = 0$, there is a slow but measurable heating of the ions due to numerical collisonality, and second, when $v_{de} \neq 0$, turbulence develops in the plasma.

Finally, the external circuit is set to a short-circuit condition: we require that $\phi(0, y) = \phi(L_x, y) = 0$ at all times.

In Fig.(2) we display the ion phase space ($v_x$vs x) at $t = 140$ ($\omega_{pi} t \approx 14$). This scatter plot shows *all* ions in the system. A large ion vortex has formed about $x =$, with a velocity trapping width of order $\Delta v_{tr} \approx 0.08 \gg v_{ti} = 0.01$. The ions in the vortex are trapped in a large-amplitude wave, which propagates in the direction of electron drift with a velocity comparable to the ion acoustic velocity $c_s = 0.1$. The two dimensional potential structure of this wave is shown in Fig.(3): this is a perspective view of the potential $\phi(x, y)$, averaged over a

time interval $T = 1.5\omega_{pi}^{-1}$ so as to suppress the high-frequency ($\omega \approx \omega_{pe} = 1$) fluctuations of the fields. Fig.(3) displays three features which are expected in this situation (,[4,5]). The first is a broad potential dip, which traps the ions observed Fig.(2). The second is a positive potential step, downstream from the ion vortex, which is formed by the asymmetric reflection of electrons by the potential dip. The third feature is a low-frequency ($\omega \leq \omega_{pi}$) turbulence, which eventually dominates the "coherent" features of the potential profile that we have just just discussed.

VI. CONCLUSION.

Further development of ES2, especially in connection with its diagnostics, will be strongly stimulated by its continued use in a number of research projects. We plan to issue a first "User's Manual" in the near future.

References

[1] *PDW1 User's Manual*, Wm. Lawson, Electronics Research Laboratory Memorandum No. UCB/ERL M84/37, 27 April 1984.

[2] *Plasma Physics via. Computer Simulation*, C.K. Birdsall and A.B. Langdon, McGraw Hill, 1985, p. 318.

[3] *Idem*, p. 312.

[4] J.S. DeGroot et al., Phys. Rev. Letters, **38**, 22 (1977) 1283.

[5] C. Barnes, M.K. Hudson, W. Lotko, Phys. Fluids, **28**, 4 (1985) 1055.

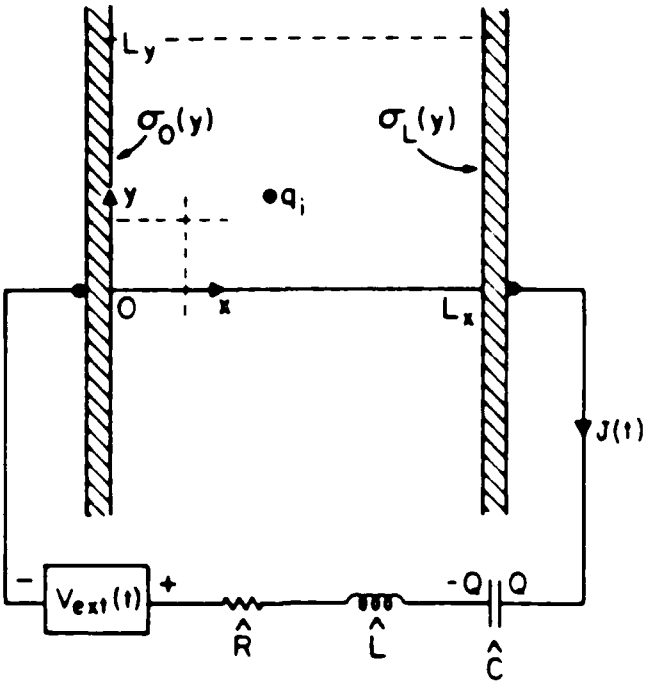

Fig.(1): General configuration of the bounded, two-dimensional simulation ES2 (this figure is copied from Plasma Physics via Computer Simulation, by C.K. Birdsall and A.B. Langdon, McGraw Hill, 1985, p.409).

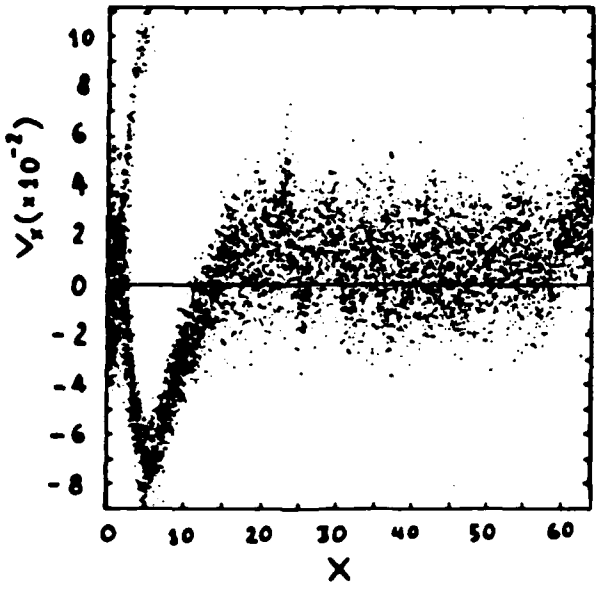

Fig.(2): Scatter-Plot of ion phase space $x-v_x$, taken at the same time as Fig.(3).

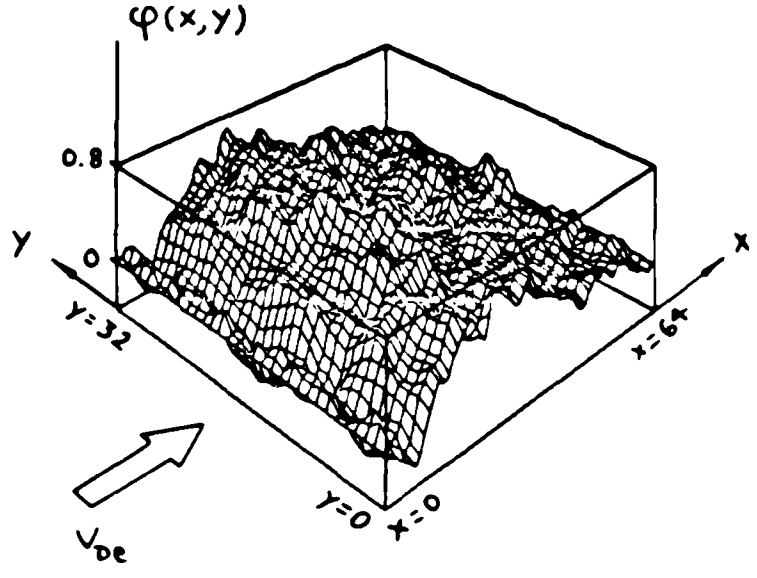

Fig.(3): Electrostatic potential at $\omega_{pe}t=100$ (time-averaged over 1.5 ω_{pi}^{-1}) from an ES2 simulation, with drifting electrons and constant injection at the walls. Parameters $v_{te}=1.0$, $v_{de}=1.0$, $v_{ti}=0.01$, $\omega_{pe}=1.0$, $m_i/m_e=100$, $\omega_{pi}=0.1$, $L_x=2L_y=64$, and no magnetic field.

time interval $T = 1.5\omega_{pi}^{-1}$ so as to suppress the high-frequency ($\omega \approx \omega_{pe} = 1$) fluctuations of the fields. Fig.(3) displays three features which are expected in this situation (,[45]). The first is a broad potential dip, which traps the ions observed Fig.(2). The second is a positive potential step, downstream from the ion vortex, which is formed by the asymmetric reflection of electrons by the potential dip. The third feature is a low-frequency ($\omega \leq \omega_{pi}$) turbulence, which eventually dominates the "coherent" features of the potential profile that we have just just discussed.

VI. CONCLUSION.

Further development of *ES2*, especially in connection with its diagnostics, will be strongly stimulated by its continued use in a number of research projects. We plan to issue a first "User's Manual" in the near future.

References

[1] *PDW1 User's Manual*, Wm. Lawson, Electronics Research Laboratory Memorandum No. UCB/ERL M84/37, 27 April 1984.

[2] *Plasma Physics via. Computer Simulation*, C.K. Birdsall and A.B. Langdon, McGraw Hill, 1985, p. 318.

[3] *Idem*, p. 312.

[4] J.S. DeGroot et al., Phys. Rev. Letters, **38**, 22 (1977) 1283.

[5] C. Barnes, M.K. Hudson, W. Lotko, Phys. Fluids, **28**, 4 (1985) 1055.

B. Energy Conserving Reflection Algorithm

Lou Ann Schwager

I. Introduction

The simulation of plasma reflecting off a boundary requires the correct formulation of an elastic reflection of a plasma ion off a wall or collector plate. Conservation of total energy at the event of reflection is crucial when, in a steady state system, particles injected at a source, traverse a potential path, perfectly reflect at a wall, and return to the origination point. In this model these particles should have no gain or loss in energy. In a real model, some of the energy of the reflected particle is imparted to the wall in inelastic reflection. Hence we provide this exercise as a reference for these cases.

During one time step of the simulation, a particle incident on a wall passes beyond it. The penetration depth depends on the previous location and present velocity of the particle. This velocity is determined with a leap-frog mover at one-half time step earlier. On reflection the position of the particle is mirrored back through the wall. As a first guess, we give the new velocity the same magnitude but opposite sign of the old velocity. This assumption does not conserve energy because the particle has been reflected across a potential difference. The following derivation provides a correction in this simply reflected velocity which includes the effect of the potential change and one-half time step correction.

II. Model

A particle of mass m, charge q, and velocity v moving along x in a time-independent electric field E has constant energy $\mathcal{E}$,

$$\mathcal{E} = \frac{mv^2}{2} - qEx. \tag{1}$$

The acceleration a on the particle is

$$a = E\left(\frac{q}{m}\right). \tag{2}$$

We assume this acceleration is constant within one spatial grid Δx of the wall and over one time step Δt prior to reflection.

If the subscript p denotes the time step prior to wall penetration, then the simulation gives us x_p and $v_{p-\frac{1}{2}}$. At the next time step when the particle is moved, the new velocity and position become

$$v_{p+\frac{1}{2}} = v_{p-\frac{1}{2}} + a\Delta t \tag{3}$$

and

$$x_{p+1} = x_p + v_{p+\frac{1}{2}}\Delta t. \tag{4}$$

If x_{p+1} exceeds the system length L and the particle is reflected (as opposed to added to the wall surface charge), then the new position and velocity are $\bar{x}_{p+1}$ and $\bar{v}_{p+\frac{1}{2}}$. We choose to reposition the particle from the wall at the distance it would have penetrated the wall.[1] Hence,

$$\bar{x}_{p+1} = 2L - x_{p+1}. \tag{5}$$

This scheme is shown in Fig. 1.

We next correct the simple velocity. The particle, first accelerated by E at the wall to x_{p+1}, is now decelerated by the same E to $\bar{x}_{p+1}$. We correct the simple velocity with δ, where

$$\bar{v}_{p+\frac{1}{2}} = -v_{p+\frac{1}{2}} + \delta. \tag{6}$$

Equating $\mathcal{E}_p$ with $\mathcal{E}_{p+1}$ determines the value for $\bar{v}_{p+\frac{1}{2}}$. This energy balance gives

$$\frac{v_p^2}{2} - ax_p = \frac{\bar{v}_{p+1}^2}{2} - a\bar{x}_{p+1}. \tag{7}$$

Second-order approximations for v^2 at the full time step are

$$v_p^2 = v_{p+\frac{1}{2}} v_{p-\frac{1}{2}} \tag{8}$$

and

$$\bar{v}_{p+1}^2 = v_{p+\frac{1}{2}} \bar{v}_{p+\frac{1}{2}} \tag{9}$$

The next velocity depends on the reflected velocity by

$$v_{p+\frac{1}{2}} = \bar{v}_{p+\frac{1}{2}} + a\Delta t. \tag{10}$$

Finally we substitute Eqs. (3)-(6) and (8)-(10) into the energy balance of Eq. (7). The solution for δ from this energy balance is in the quadratic equation:

$$0 = \delta^2 + \delta\left(a\Delta t - 2v_{p+\frac{1}{2}}\right) + 4a\left(x_{p+1} - L\right) - 2av_{p+\frac{1}{2}}\Delta t. \tag{11}$$

To evaluate δ, we consider the ordering of terms in Eq. (11). Because the leap-frog mover estimates position and velocity through a first-order central difference, these approximations (Eqs. (3), (4), and (10)) are of $O\left((\Delta t)^3\right)$.[2] Simple reflected velocity is $O(1)$ because as $\Delta t \to 0$, then $x_{p+1} \to L$ and $\bar{v}_{p+\frac{1}{2}} \to -v_{p+\frac{1}{2}}$. Finally the v^2 approximation in Eqs. (8) and (9) introduces an error with $O\left((\Delta t)^2\right)$, which then is the lowest-order error of Eq. (11). This determines that δ is $O(\Delta t)$. If we neglect terms with $O\left((\Delta t)^2\right)$ or greater, then the second-order approximation for δ becomes

$$\delta = \frac{2a}{v_{p+\frac{1}{2}}}(x_{p+1} - L) - a\Delta t. \tag{12}$$

Note that for no wall charge, $a = 0$, and so $\bar{v}_{p+\frac{1}{2}} = -v_{p+\frac{1}{2}}$.

III. Conclusion

The maximum wall penetration, $x_{p+1} - L = v_{p+\frac{1}{2}}\Delta t$, fixes δ at $+a\Delta t$. Minimum penetration, $x_{p+1} = L$, generates the smallest correction with $\delta = -a\Delta t$. Because the value

of x_{p+1} is equally probable across the range from L to $L+v_{p+\frac{1}{2}}\Delta t$, the average value of δ after many reflections is zero. On the other hand, the correction δ generates a spread in velocities of the reflected ions. Consequently, if a substantial electric field develops at the wall and we use only simple reflection, the reflected ion flux would be erroneously cooled.

Typically for a low temperature plasma, the wall absorbs about 20% of the incident particle energy. The specific fraction depends on the mass ratio of the incident particle and wall target.[3] For this example, the velocity of the reflected particle is about 90% of its incident velocity. Specifically in the simulation the new reflected velocity would be

$$\bar{v}_{p+\frac{1}{2}} = -0.9\, v_{p+\frac{1}{2}} + \delta. \tag{13}$$

IV. Acknowledgment

We give special thanks to Bill Lawson who contributed to the ideas presented here.

References

[1] C. K. Birdsall and A. B. Langdon, *Plasma Physics via Computer Simulation*, McGraw-Hill, New York, (1985), p.142.

[2] J. F. Botha and G. F. Pinder, *Fundamental Concepts in the Numerical Solution of Differential Equations*, Wiley, New York, (1983), p.25.

[3] R. A. Langley *et al*, "Data Compendium for Plasma-Surface Interactions", *Nuclear Fusion* special issue, (1984), pp.12–27.

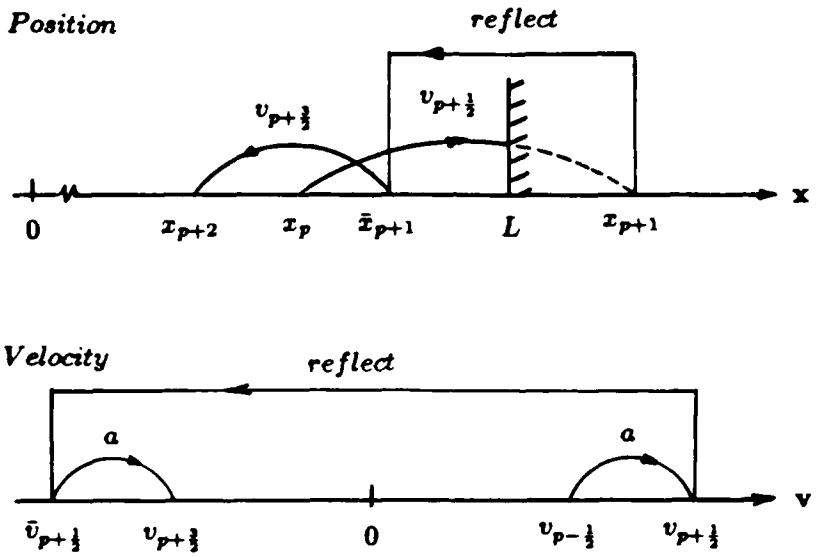

Figure 1. Position and velocity of particle before, during, and after reflection.

SECTION IV: JOURNAL ARTICLES, REPORTS, TALKS, VISITS

Journal Articles

T. L. Crystal and S. Kuhn, "Particle Simulations of the low-α Pierce Diode," Phys. Fluids 28 (7), July 1985, pp. 2116-2124.

V. A. Thomas, V. M. Nevins, Y. J. Chen, "Simulation of the ion-beam-driven drift instability in a magnetic trap. I," Phys. Fluids 28 (7), July 1985, pp. 2235-2247.

V. A. Thomas, V. M. Nevins, "Simulation of the ion-beam-driven drift instability in a magnetic trap. II," Phys. Fluids 28 (7), July 1985, pp. 2248-2257.

W. S. Lawson, "A Method for Simulation of Vlasov Systems with Discontinuous Distribution Functions," Journal of Computational Physics, Vol. 61, No. 1, October 1985, p. 51.

Reports

C. K. Birdsall, T. L. Crystal, P. C. Gray and S. Kuhn, "Bounded Plasma Dynamics from Particle Simulations; movie script," UCB/ERL M85/54, 2 July 1985.

Talk at INTOR, Technical Experts Meeting on Impurity Control Modelling, Vienna, 16-18 Sept 1985:

C. K. Birdsall, "Boundary Conditions; Matching plasma-sheath-wall."

Poster papers at the Twenty-Seventh Annual Meeting, Division of Plasma Physics, San Diego, November 4-8, 1985 (abstracts follow)

B. I. Cohen, M. E. Stewart, R. P. Freis, C. K. Birdsall, "Direct Implicit Particle Simulation of Tandem Mirrors"

K. Theilhaber, G. Laval, D. Pesme, "Simulations of the Beam-Plasma Instability in the Turbulent-Trapping Regime"

M. Oertl, P. Krumm, S. Kuhn, "Single Ended Q-Machine Equilibria--Experiment vs. Theory"

P. C. Gray, T. L. Crystal, S. Kuhn, C. K. Birdsall, "Equilibrium Corrections for Electron Hole filling: Simulation vs. Theory"

C. K. Birdsall, P. C. Gray, T. L. Crystal, "A Simulation Study of the Dependence of the Plasma Sheath Impedance on Frequency"

L. A. Schwager, C. K. Birdsall, "A Model of the Plasma-Sheath Region Including Secondary Electron Emission and Ion Reflection"

A. Wendt, P. C. Gray, H. Meuth, M. A. Lieberman, C. K. Birdsall, "Experimental and Simulation Study of Planar Magnetron Discharges"

Wm. Lawson, P. C. Gray, E. A. Adler, C. K. Birdsall, "A Simulation Study of Effects of Emmission Noise in a Thermionic Diode"

Direct Implicit Particle Simulation of Tandem Mirrors.* B. I. COHEN, M. E. STEWART, and R. P. FREIS, *Lawrence Livermore National Laboratory*, and L. A. STRUGALA and C. K. BIRDSALL, *University of California, Berkeley* - TESS is a one-dimensional axial particle code for simulating thermal-barrier formation and loss of plugging in a tandem mirror plasma. TESS calculates the self-consistent ambipolar potential from data collected from advancing particle ion and electron trajectories from the midplane of the center cell to the end of the device. By performing a direct implicit solution for the electric potential, we are allowed to use a long time step. An accurate representation of passing and trapped, relativistic electron and ion guiding-center dynamics is rendered by conventional particle simulation and Monte Carlo techniques. Charge exchange and ionization processes are represented probabilistically. The wave heating effects of ECRH and ICRF are modeled with the quasilinear formalism of Bernstein and Baxter. Transit loss and self-consistent binary Coulomb collisions that conserve energy and momentum are included. A probability for radial loss is calculated analytically for classical and neoclassical radial transport.

---

* Work performed for U.S.D.O.E. by Lawrence Livermore National Laboratory under contract W-7405-ENG-48.

Simulations of the Beam-Plasma Instability in the Turbulent-Trapping Regime, K. THEILHABER, U.C. Berkeley, G. LAVAL and D. PESME, Ecole Polytechnique, France, -- In the weak warm-beam-plasma instability, the "turbulent-trapping" regime[1] is defined by $\nu = (k^2 D)^{1/3} > \gamma_k$ where γ_k is the growth-rate and ν the resonance-broadening frequency. In this regime, trapping dominates the phase-space structure of the distribution function, leading to the generation of a harmonic series of quasimodes resonant with the beam particles, and to a theoretical increase of growth-rates and diffusion above the quasilinear values. While our simulations confirm the detailed structure of the correlation functions predicted by the turbulent-trapping theory, they do not show the expected enhancement of the growth-rates. We shall discuss these results, and link them to a numerical study of velocity-space diffusion in the turbulent fields. This will lead to a revision of the Fokker-Planck equation for the correlation function.

1. G. Laval and D. Pesme, Phys. Rev. Lett., 53,3, 270 (1984).

Supported by DOE Contract DE-AT03-76ET53064 and ONR Contract N00014-77-C-0578.

Single Ended Q Machine Equilibria - Experiment vs. Theory.* M. OERTL, P. KRUMM, and S. KUHN, Innsbruck University, Austria.--Equilibrium studies of the single ended Q machine with negatively biased cold plate, based on a collisionless plane diode model, have predicted[1] that, for increasing q (neutral flux towards the hot plate), both n_e (plasma density) and j_i (ion current density) should first increase monotonically (regime 1', monotonically decreasing potential profile); after reaching some "transition point", n_e should decrease slightly while j_i should remain almost constant (regime 2', potential profile with maximum near the hot plate). In the present experiment, this prediction has been checked by monitoring n_e and j_i while increasing q, for differnt values of the hot plate temperature T. While regime 1' and the transition point are recovered in accordance with theory, regime 2' shows strongly increasing j_i and slightly increasing n_e. This evidence, along with recent simulation results,[2] suggests a slight modification of the theory so as to allow for trapped electrons in the region of the potential maximum near the hot plate.

*Work supported by Austrian Research Funds Contracts S-18/02, S-18/03, and P5178.

[1]S. Kuhn, Plasma Phys. 23, 881 (1981)
[2]S. Kuhn et al., Proceedings of the 1984 Int. Conf. on Plasma Physics, Lausanne, Contributed Papers, p. 104.

Equilibrium Corrections for Electron Hole Filling: Simulation vs. Theory , P. C. GRAY, T. L. CRYSTAL, S. KUHN* and C.K. BIRDSALL, U.C. Berkeley--A recent quantitative theory for axial one dimensional equilibria of a collisionless single-ended Q-machine predicts the maximum and plasma potential for the case when the considered particle source is taken ion rich and the over all bias is held negative[1]. In this case a single positive potential extremum is near the cathode and the steady state theory assumes an electron hole in phase space from which all electrons are forbidden. However, particle simulations of this bounded-plasma configuration recover very different values of potential, and the assumed electron hole is found to be filled in[2]: the electron distribution $f(v,x)$ is measured to be Maxwell-Boltzmann, $f(\phi,x)$. This result may also explain some recent equilibrium measurements[3].-- Work supported by DOE Contract DE-AS03-76-F00034-DE-AT03-76ET53064, ONR Contract N00014-77-C-0578 and Austrian Research Funds. Simulations performed at NMFECC.

1. Kuhn, S.,Plasma Phys., Vol. 23, pp. 881-902, 1981.
2. Kuhn, S., Proc. I.C.P.P., Lausanne Swi., Vol. 1, pp. 104, June 1984.
3. Oertl, M. et al., this conference.

*Innsbruck University, Austria.

A Simulation Study of the Dependence of the Plasma Sheath Impedance on Frequency, C. K. BIRDSALL, P. C. GRAY and T. L. CRYSTAL, U. C. Berkeley--
A one dimensional electrostatic particle code bounded with an external circuit[1] has been used to model the parallel sheath. Static potential profiles agree with simple Boltzmann electron theory. The model has been used to measure the frequency dependence of the sheath-impedance about the floating potential, for frequencies $0< \omega < 5\omega_{pe}$. The impedance includes effects from potential drops at both the plasma source and the collector. For a short system at low frequency the impedance appears resistive, with $R_{10} = 1/g_{10}$ where g_{10} is obtained from dc measurement of $\partial J/\partial \phi$ at the floating potential. A parallel resonance is found at $\omega = \omega_{pe}$ of the plasma region, due to the vacuum C of bounded system and L associated with electron inertia. It is necessary to shunt the sheath resistance with a large capacitance in order to account for the ion imobility at $\omega \lesssim \omega_{pi}$. The overall result is an approximate RLC equivalent circiut for the sheath. For a longer system, $\phi^2(x)$ for various choices of driving frequency has been computed showing the spatial behavior of the signal.--Work supported in part by DOE contract DE-AS03-76-F00034-DE-AT03-76ET53064, ONR contract N00014-77-C-0578 and a gift from Varian Associates.

1. Wm. Lawson, U.C. Berkeley, Memorandum No. UCB/ERL M84/45, June 13, 1984.

A Model of the Plasma-Sheath Region Including Secondary Electron Emission and Ion Reflection. L.A. Schwager, C.K. Birdsall, Electronics Research Lab, U.C. Berkeley.*--The interaction of a medium temperature plasma with a collector plate is studied allowing emission of secondary electrons and reflection of plasma ions. These effects alter the electrostatic potential drop across the sheath region and plasma transport to the plate. The computer code PDW1 models this behavior, solving for particle motion in the self-consistent electrostatic field, in one-dimension. Particle ions and electrons, which are injected continuously from a hot plate into a plasma region, flow to a floating plate which reflects ions or emits secondary electrons. Our ion reflection simulation results compare well with our static cold ion theory. We also observe an ion-ion two-streaming instability as predicted by our time-dependent theory. Our secondary electron results compare well with previous theory and demonstrate charge saturation as predicted.[1]
*Supported by DOE contract DE-AT03-76ET53064.
[1]G.D. Hobbs and J.A. Wesson, Plasma Physics, Vol.9, (1967).

Experimental and Simulation Study of Planar Magnetron Discharges* A. WENDT, P.C. GRAY, H. MEUTH, M.A. LIEBERMAN and C.K. BIRDSALL, U. C. Berkeley--
An apparatus has been constructed for investigation of plasma processes in planar magnetron discharges. Objectives include finding the mechanisms and values of ion acceleration and electron current, as well as the role of waves and fluctuations. The experiment consists of independently positioned, moveable parallel plate electrodes in a cylindrical chamber and diagnostics that allow for axially as well as radially resolved measurements of temperature, density and fluctuations. We are also using an electrostatic bounded particle code (1 space, 3 velocity dimensions) to simulate the magnetron discharge. The code includes modeling of bulk ionization and electron-neutral collisions. Comparision of preliminary experimental measurements and simulation results will be given.
*Research supported by a gift from Varian Associates.

A Simulation Study of Effects of Emission Noise in a Thermionic Diode , Wm. LAWSON, P. C. GRAY, E. A. ADLER*and C. K. BIRDSALL, U. C. Berkeley --
The transition between the space-charge-limited and temperature-limited operating regimes of a thermionic diode is not well understood. It has been found experimentally that the current-voltage-temperature characteristic fits a simple universal formula[1]. The wide spread applicability of this formula suggests that the physics of the transition involves some universal mechanism; it is not solely a question of the surface properties of the emitter. It has been suggested that the interaction of emission noise with the space-charge cloud just outside the cathode surface may affect the observed dc current-voltage characteristic near the transition. This effect has been studied using the PDW1 simulation code[2]. We will discuss the effect of varying levels of emission noise on both the current-voltage characteristics and the dynamics of the potential minimum.--Work supported in part by Hughes Aircraft Company.
1. R.T. Longo, IEDM 1978, p.152.
2. Wm. Lawson, U. C. Berkeley, Memorandum No. UCB/ERL M84/45, June 13, 1984.
*Hughes Aircraft Company, Torrance.

DISTRIBUTION LIST

Argonne National Laboratory
Brooks

Austin Research Associates
Roberson

Bell Telephone Laboratories
Hasegawa

Berkeley Research Assoc.
Brecht, Orens, Thomas

Berkeley Scholars, Inc.
Ambrosiano

Bhabha Research Centre
Gioel

Cal. Inst. of Technology
Bridges, Gould, Liewer

Cal. State Polytech. Univ.
Rathmann

Cambridge Research Labs.
Rubin

Centro de Electrodinamica, Lisbon
Brinca

Columbia University
Chua

Culham Laboratory
Eastwood

Dartmouth
Crystal, Hudson, Lotko

Department of Energy
Hitchcock, Macrusky, Nelson, Sadowski

Ecole Polytechnique, Lausanne
Hollenstein

Ecole Polytechnique, Palaiseau
Adam

E.P.R.I.
Scott

Ga Technologies
Evans, Helton, Lee

Hascomb Air Force Base
Rubin

Hewlett-Packard Laboratories
Gleason, Moreoux

Hiroshima University
Tanaka

Hughes Aircraft Co., Torrance
Adler, Longo

Hughes Research Lab., Malibu
Harvey, Hyman, Poeschel, Schumacker

I.N.P.E.
Bittencourt, Montes

Institute of Fusion Studies
Librarian

IPP-KFA
Reiter

JAYCOR
Hobbs, Tumolillo

Kirtland Air Force Base
Pettus

Kyoto University
Abe, Jimbo, Matsumoto

Lawrence Berkeley Laboratory
Cooper, Kaufman, Kunkel, Lee

DISTRIBUTION LIST (cont.)

Lawrence Livermore National Laboratory

Albritton, Anderson, William Barr, Brengle, Bruijnes, Byers, Chambers, Chen, B. Cohen, R. Cohen, Denavit, Estabrook, Fawley, Fowler, Friedman, Fries, Fuss, Hewett, Killeen, Langdon, Liasinski, Matsuda, Max, Nevins, Nielsen, Smith, Tull

Massachusetts Institute of Technology

Berman, Bers, Gerver, Lane

Max Planck Inst. für Plasmaphysik

Biskamp, Chodura

Mission Research Corporation

Godfrey, Mostrom

Nagoya University

Kamimura, Research Info. Center

Naval Research Laboratory

Boris, Haber, Joyce, Winsor

New York University

Grad. Harned, Otani, Weitzner

Northeastern University

Chon, Silevitch

Oak Ridge National Lab.

Fusion Energy Library, Meier, Mook

Osaka University

Mima, Nishihara

Oxford University

Allen, Benjamin

Princeton Plasma Physics Lab.

Chen, Cheng, Lee, Okuda, Tang

Physics International

Woo

Riso National Laboratories

Lynov, Pecseli

SAI Corporation - Boulder

D'Ippolito, Myra

SAI Corporation - Palo Alto

Siambis

SAI Corporation - Virginia

Drobot, Mankofsky, McBride, Smith

Sandia Labs, Albuquerque

Freeman, Poukey, Quintenz, Wright

Shizuoka University

Saek

Stanford University

Blake, Buneman, Gledhill, Physics Library, Storey

Tel Aviv University

Cuperman

Tohoku University

N. Sato

TRW

Wagner

University of Arizona

Morse

Universität Bochum

Bochum

University of California, Berkeley

Arons, Birdsall, Chorin, Haller, Hess, Lawson, Lichtenberg, Lieberman, Morse, Theilhaber, Wendt

University of California, Davis

DeGroot

DISTRIBUTION LIST (cont.)

University of California, Irvine
Rynn

Universität Innsbruck
Cap, Kuhn

University of Iowa
Knorr, Nicholson

Universität Kaiserslautern
Wick

University of Maryland
Gillory, Rowland

University of New Mexico
Anderson, Humphries

University of Pittsburgh
Zabusky

University of Southern California
Kuehl

University of Texas
Horton, Lebouef, McMahon, Tajima

University of Toronto
Stangeby

University of Tromso
Armstrong, Trulsen

Varian Associates
Helmer

NEW LISTINGS SINCE LAST DISTRIBUTION:

Fusion Technology Institute
Emmert, Gilbert A.

Imperial College
Burger, Peter

University of California, Los Angeles
Prinja, Anil

University of Iowa
Knorr, Nicholson

University of Wisconsin
Hershkovitz, Intrator

Varian Associates
Anderson, Weston

END

5-87

DTIC